



**Hydrodynamic and morphodynamic impacts of a flood
discharge tunnel in the Tagus estuary**

Modelling the local effects

Pedro Miguel Parreira Russo da Costa e Vasconcelos

Thesis to obtain the Master of Science Degree in

Environmental Engineering

Supervisor: Prof. Dr. Marcos Duarte Mateus

Examination comitee:

Chairperson: Prof. Dr. José Manuel de Saldanha Gonçalves Matos

Supervisor: Prof. Dr. Marcos Duarte Mateus

Members of the Comitee: Prof. Dr. Lígia Laximi Machado de Amorim Pinto

September 2017

Acknowledgements

This work was made possible only with the help, directly or otherwise, of a number of people, and I would like to thank them for their contribution.

My profoundest gratitude to Prof. Doctor Marcos Duarte Mateus for his guidance, supervision and assistance, without which this work would have been impossible.

My sincerest appreciation to Guilherme Franz, the person who developed the sediment module used in this thesis, for his helpfulness and patience in teaching me how to use it and for his help with solving errors.

Thanks to all my friends for their support and encouragement. This thesis has been a most difficult task in my student career, and their continued care and motivation was fundamental.

My deepest thank you to my girlfriend, Rita, for being the most caring and loving person I know, and who always encouraged me to keep going and to do and be the best I can.

Abstract

Due to frequent flooding in Lisbon, in particular in the lower areas such as Alcântara and Chelas, and the recent worsening of these floods because of climate change and increasing population, there is a need to develop solutions that reduce the impacts, the causes or the frequency of flooding. One such measure, as outlined in the General Drainage Plan for Lisbon 2016 - 2030 (*Plano Geral de Drenagem de Lisboa 2016 - 2030* or PGDL) is the construction of a rainwater drainage tunnel which would collect excessive or flooding rain water and discharge it in the Tagus river's estuary, designed to drain emergency water loads that the standard drainage system currently in place is not able to handle.

Using a numerical modelling software (MOHID), this tunnel's discharge was simulated, with the goal of predicting potential hydrodynamic (changes to the velocity field and modulus and dispersion of a generic conservative pollutant) and morphodynamic (changes to the estuary's bathymetry, sediment dispersion) impacts on the Tagus river's estuary.

The simulated results suggest that hydrodynamic impacts are both localized and temporary, as 2 hours after the discharge stops, the effects are very small or negligible, whereas during the discharge, the approximate maximum radius of the affected area is 1150m. As for the morphodynamic impacts, the effects of the discharge are very low throughout the simulation, as the discharge doesn't occur at a sufficient enough depth to significantly affect the bottom. Therefore, these impacts, as simulated, are considered to have a low significance in the general context of the PGDL.

Keywords: modelling, hydrodynamic, morphodynamic, impacts, sediments, floods

Resumo

Devido à frequência de situações de cheias em Lisboa, particularmente nas zonas baixas de Alcântara e Chelas, e ao agravamento recente destas situações devido às alterações climáticas e à crescente população, verifica-se a necessidade de desenvolver soluções que permitam reduzir os impactos, causas ou frequência das cheias. Para tal, uma possível medida prevista no Plano Geral de Drenagem de Lisboa 2016 - 2030 (PGDL) que permita essa redução de impacto é a criação de um túnel de drenagem de águas pluviais, que recolha caudais de águas pluviais em regime de emergência, ou seja, que o sistema de escoamento actual não consiga dar resposta, e que descarregue no estuário do rio Tejo.

Utilizando um modelo numérico (MOHID), simulou-se a descarga deste túnel, com o objectivo de prever potenciais impactos hidrodinâmicos (alteração ao módulo e ao campo de velocidades e dispersão de um poluente genérico discreto conservativo) e morfodinâmicos (alteração da batimetria do estuário, dispersão de sedimentos) ao estuário do rio Tejo.

Os resultados simulados indicam que os impactos ao nível hidrodinâmico são locais e temporários, uma vez que após 2 horas do término da descarga, os seus efeitos são vestigiais ou desprezáveis; por outro lado, durante a descarga, o raio máximo da área afectada é de aproximadamente 1150m. Quanto aos impactos morfodinâmicos, os efeitos da descarga a este nível são muito baixos durante toda a simulação, já que a descarga não ocorre a uma profundidade suficiente para que os seus efeitos se façam sentir no fundo. Assim sendo, os impactos simulados são considerados de pouca importância no contexto geral do PGDL.

Palavras-chave: modelação, hidrodinâmica, morfodinâmica, impactos, sedimentos, cheias

Table of Contents

1. Introduction.....	1
1.1 Motivation.....	1
1.2 Context.....	1
1.3 Objectives.....	2
2. Literature review.....	4
2.1 Flooding in Lisbon.....	4
2.2 Description of the estuary.....	5
2.3 Description of the discharge tunnel.....	6
3. Methodology.....	9
3.1 The Mathematical Model.....	9
3.2 Model setup.....	12
3.2.1 Location.....	13
3.2.2 Bathymetry.....	14
3.2.3 Model parametrization.....	16
3.3 Results' analysis.....	20
4. Results.....	22
4.1 Hydrodynamics.....	22
4.1.1 Velocity modulus, velocity field and water level.....	22
4.1.2 Water properties.....	34
4.2 Morphodynamics.....	41
4.2.1 Shear stress.....	42
4.2.2 Cohesive sediments.....	43
4.2.2 Sand classes.....	46
5. Conclusions and future work.....	51
6.1 Conclusions.....	51
6.2 Future work.....	52
References.....	54
Annexes.....	57

Index of Figures

Figure 1 - Example of the 2014 floods in Lisbon. (Pincha et al. 2014).....	4
Figure 2 - Lisbon Municipality's flood risk vulnerability map.....	5
Figure 3 - Satellite photograph of the Tagus estuary.....	6
Figure 4 - General outline of the discharge tunnel, in yellow. (PGDL, 2015).....	7
Figure 5 - Sediment module's model layers and associated processes. The different shades in the settled layer represents sediment stratigraphy. (Franz et al. 2017).....	12
Figure 6 - Approximate location of the "main" model's geographical extent.....	13
Figure 7 - Approximate location of the "nested" model's geographical extent.....	14
Figure 8 - "main" model grid over Lisbon's coastline.....	15
Figure 9 - "nested" model grid over Lisbon's coastline.....	15
Figure 10 - "main" model bathymetry.....	16
Figure 11 - "nested" model bathymetry.....	16
Figure 12 - Locations for the time series for the "main" model, in dark red.....	17
Figure 13 - Locations for the time series for the "nested" model, in dark blue.....	18
Figure 14 - Velocity modulus (m/s) and field at 00:00:00, "main" model, horizontal map image.....	23
Figure 15 - Velocity modulus (m/s) and field at 00:00:00, "main" model, vertical cut image.....	24
Figure 16 - Velocity modulus (m/s) and field at 01:10:00, "main" model, horizontal map image.....	24
Figure 17 - Velocity modulus (m/s) and field at 01:10:00, "main" model, vertical cut image.....	25
Figure 18 - Velocity modulus (m/s) and field at 03:30:00, "main" model, horizontal map image.....	25
Figure 19 - Velocity modulus (m/s) and field at 03:30:00, "main" model, vertical cut image.....	26
Figure 20 - Velocity modulus (m/s) and field at 07:00:00, "main" model, horizontal map image.....	26
Figure 21 - Velocity modulus (m/s) and field at 07:00:00, "main" model, vertical cut image.....	27
Figure 22 - Velocity modulus (m/s) and field at 10:10:00, "main" model, horizontal map image.....	27
Figure 23 - Velocity modulus (m/s) and field at 10:10:00, "main" model, vertical cut image.....	28
Figure 24 - Velocity modulus (m/s) and field at 11:10:00, "main" model, horizontal map image.....	28
Figure 25 - Velocity modulus (m/s) and field at 11:10:00, "main" model, vertical cut image.....	29
Figure 26 - Velocity modulus (m/s) and field at 12:00:00, "main" model, horizontal map image.....	29
Figure 27 - Velocity modulus (m/s) and field at 12:00:00, "main" model, vertical cut image.....	30
Figure 28 - Velocity modulus (m/s) and water level over time, "main" model, south-west domain border locations.....	31
Figure 29 - Velocity modulus (m/s) and water level over time, "main" model, centre of the domain and tunnel mouth locations.....	31
Figure 30 - Velocity modulus (m/s) and field at 10:10:00, "nested" model, horizontal map image.....	32
Figure 31 - Velocity modulus (m/s) and field at 11:10:00, "nested" model, horizontal map image.....	32
Figure 32 - Velocity modulus (m/s) and field at 12:00:00, "nested" model, horizontal map image.....	33
Figure 33 - Velocity modulus (m/s) and water level over time, "nested" model, south-west domain border locations.....	34
Figure 34 - Velocity modulus (m/s) and water level over time, "nested" model, centre of the domain and tunnel mouth locations.....	34

Figure 35 - Generic conservative property concentration at 03:30:00, "main" model, horizontal map image.....	36
Figure 36 - Generic conservative property concentration at 03:30:00, "main" model, vertical cut image.....	36
Figure 37 - Generic conservative property concentration at 07:30:00, "main" model, horizontal map image.....	37
Figure 38 - Generic conservative property concentration at 07:30:00, "main" model, vertical cut image.....	37
Figure 39 - Generic conservative property concentration at 09:30:00, "main" model, horizontal map image.....	38
Figure 40 - Generic conservative property concentration at 12:00:00, "main" model, horizontal map image.....	38
Figure 41 - Generic conservative property concentration at 12:00:00, "main" model, vertical cut image.....	39
Figure 42 - Generic conservative property concentration over time, "main" model, north-east domain border locations.....	39
Figure 43 - Generic conservative property concentration over time, "main" model, all locations except north-east border locations and tunnel mouth.....	40
Figure 44 - Generic conservative property concentration at 12:00:00, "nested" model, horizontal map image.....	40
Figure 45 - Generic conservative property concentration at 06:30:00, "nested" model, vertical cut image.....	41
Figure 46 - Generic conservative property concentration at 10:10:00, "nested" model, vertical cut image.....	41
Figure 47 - Bottom shear stress at 03:40:00, horizontal map image.....	42
Figure 48 - Bottom shear stress at 05:50:00, horizontal map image.....	43
Figure 49 - Bottom shear stress at 12:00:00, horizontal map image.....	43
Figure 50 - Fluid mud layer at 00:40:00.....	44
Figure 51 - Fluid mud layer at 06:00:00.....	45
Figure 52 - Fluid mud layer at 06:40:00.....	45
Figure 53 - Fluid mud layer at 07:40:00.....	46
Figure 54 - Fluid mud layer at 12:00:00.....	46
Figure 55 - Concentration of very fine (class 1) sand at 03:40:00, horizontal map image.....	47
Figure 56 - Concentration of very fine (class 1) sand at 03:40:00, vertical cut image.....	48
Figure 57 - Concentration of very fine (class 1) sand at 05:50:00, vertical cut image.....	48
Figure 58 - Concentration of very fine (class 1) sand at 12:00:00, vertical cut image.....	49

Index of Tables

Table 1 - Coordinates of "main" and "nested" models' domains.....	14
Table 2 - ID, locations and coordinates for the time series' locations.....	18
Table 3 - Sand classes, with d_{50} being the median diameter of each class, considered to be the representative diameter of each class.....	19

Annexes

Annex A - Flood discharge tunnel's layout, first half.....	57
Annex B - Flood discharge tunnel's layout, second half.....	58
Annex C - Flood discharge tunnel's mouth's technical drawing.....	59

List of Symbols

p_{atm}	Atmospheric pressure
f	Coriolis parameter
ρ	Density
d	Distance
η	Free surface level
k_h	Horizontal turbulent diffusivity
ν_h	Horizontal turbulent viscosity
u	Horizontal velocity in x
v	Horizontal velocity in y
p	Pressure
A	Property
ρ_0	Reference density
S	Salinity
S_i	Sinks
S_0	Sources
T	Temperature
z	Vertical coordinate
k_v	Vertical turbulent diffusivity
ν_v	Vertical turbulent viscosity
w	Vertical velocity in z

1. Introduction

1.1 Motivation

The subject for this work arose from a personal interest in working with mathematical modelling tools, as well as from the notion that modelling has become an important method of gathering information for prediction analysis. In particular, the sediment model used in this work is a very recent development in the field of computer modelling, and this work also shows its potential and limitations. Furthermore, sediment models are, in general, fairly new within the modelling “milieu”, and any opportunity to test them may be of interest for the scientific community at large.

Moreover, modelling as a scientific tool has a bright future and will only grow from here on out, as computers become more efficient and models more refined and detailed; as such, I believe it may open professional possibilities for my own career. This is further compounded by the fact that the object of this thesis is a real project being developed by the Lisbon Municipality rather than some nebulous or abstract study.

1.2 Context

This work’s ultimate interest and value comes from the fact that it may present some insight into possible future solutions to a very present problem: flooding due to extreme rainfall events in Lisbon. These events are frequent and drastic enough that they have resulted in infrastructural problems within the city, and it is clear that effective solutions must be found.

The publicly available document, *Plano Geral de Drenagem de Lisboa 2016 - 2030* (henceforth referred to as PGDL), outlines possible solutions to this and other drainage problems. The plan that this report relates to was developed by the Lisbon Municipality as a means to create a better drainage infrastructure with which to tackle not just the historically known issues with drainage within the city, but also future problems which may come from the exacerbation of current trends in terms of coping with worsening climatic conditions.

While this work is presented as merely a theoretical model of a real possible solution put forth by the PGDL report, and therefore isn’t meant to be taken as a thorough and *de facto* study of that particular solution’s feasibility, it may, in the long term, contribute to the broader discussion about how to improve urban development and planning with regards to risk management in Lisbon. This is an issue that will be characterized over the next chapter.

1.3 Objectives

The ultimate goal of this thesis is to determine the existence or absence of a localized impact associated with the aforementioned tunnel's discharge and to determine the degree to which this discharge may alter the physical conditions of the affected area, which is to be achieved by computer modelling. In order to do that, this work was structured in the following sequential steps:

- Acquisition of base data - description of relevant structures and their interactions, such as the tunnel and the estuary;
- Model implementation - setting up the modelling domain for the study area and the nested local domain for the discharge site;
- Running the model - hydrodynamic and morphodynamic model simulations;
- Impact study - assessing potential hydrodynamic and morphodynamic impacts of the discharge.

2. Literature review

2.1 Flooding in Lisbon

Lisbon has a history record of several flooding events. According to *DISASTER - GIS database on hydro-geomorphological disasters in Portugal*, in the period of 1865 up to 2010, there have been 411 documented occurrences of floods in the Lisbon metropolitan area. According to the same source, this district accounts for 25.3% of all flooding events with damaging effects (deaths, evacuees and dislodged people) in the aforementioned period in Portugal. It is important to note, however, that according to the DISASTER GIS, the number of flooding events appears to be steadily decreasing since around 1965, with significant (but also decreasing) peaks approximately every 15 years.

However, it is also important to note that there are factors that have somewhat worsened the effects of rainfall and climatic events in Lisbon, such as poor city planning, soil sealing, and potential effects related to climate change, and therefore the foreseeable future might bring more impactful floods. It is likely that the biggest contributor to the worsening of the impact of flooding in Lisbon is indeed the degree of soil sealing, which is the fourth in European capitals in percentage of urban morphological zone (behind only Warsaw, Tirana and Bucharest) at 105m² of sealed soil per capita (European Environment Agency, 2011).

The most recent significant flooding event in Lisbon occurred in 2014, when several locations throughout Lisbon city proper were hit by intense rainfall to the point where many buildings (including both shops and housing), vehicles (motorcycles and cars) and other infrastructure (such as subway lines) were heavily damaged, as seen in Figure 1.



Figure 1 - Example of the 2014 floods in Lisbon. (Pincha et al. 2014)

Indeed, according to Lisbon Municipality's flood risk vulnerability map (Carta de vulnerabilidade ao risco de inundação no Concelho de Lisboa), many areas within the city are subject to a high risk of flooding, with many more being subject to a medium risk, as seen in Figure 2.



Figure 2 - Lisbon Municipality's flood risk vulnerability map.

Over time, because of Lisbon's vulnerability to extreme precipitation and floods, and of the threat of the impacts of those events becoming more negative and significant, it has become obvious that there is a need to adopt strategies to minimize the impact from flooding events in Lisbon.

2.2 Description of the estuary

The location being studied is the Tagus river's estuary. It marks the transition between the Tagus river and the Atlantic ocean, and therefore it is affected by both bodies of water's dynamics. Its size is about 320km², its width varies between 2 and 15 km, its average depth is 10.6m and it is approximately 80km long (Fernandes 2005). The estuary's geographic upper limit is located near Muge. According to Rodrigues (2015), the tidal influence is extremely important in the estuary dynamics: the tidal prism is around 600×10⁶m³ while the river flow per tidal cycle is 8.2×10⁶m³, and there is a 4000ha difference in

submerged area between high and low tides. The main source of fresh water is the Tagus river with an average water flow of around $300\text{m}^3/\text{s}$, but there is a considerable monthly and seasonal variability. The general location of the Tagus river's estuary is displayed in Figure 3.

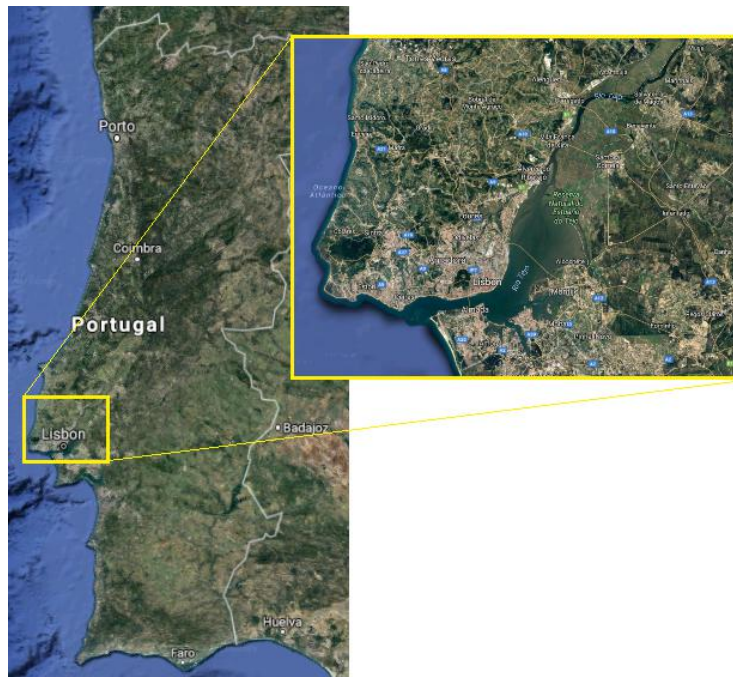


Figure 3 - Satellite photograph of the Tagus estuary.

2.3 Description of the discharge tunnel

The General Draining Plan for Lisbon 2016-2030 (Plano Geral de Drenagem de Lisboa 2016-2030), or PGDL, is a plan developed for the Municipality of Lisbon with the intention of developing an “integrated solution for flood control, endowing the city of Lisbon with a set of drainage infrastructures that would allow it to face the challenges of the 21st century”. Its goal is also “minimizing social and environmental impacts of floods, integrating all projected actions with the Municipal Director Program (Programa Director Municipal, PDM), good policies in regards to climatic adaptation and other projected actions from other city development plans” (PGDL, 2015).

One of the proposed measures outlined in the PGDL is the construction of a flood discharge tunnel (described below). Information regarding this tunnel's discharge served as the basis for this thesis. It is important to note, however, that this study concerns only the potential hydrodynamic and morphodynamic impacts of such a discharge on the Tagus river's estuary; therefore, the design of the tunnel before the discharge site, i.e. where it originates or what path it follows to the discharge site, are not factored in this work and as such will not be studied.

As mentioned, the subject of this work is the discharge of a flood discharge tunnel, about 5km long, originating roughly in the Monsanto area and discharging in the Sta. Apolónia area. It has slopes ranging from 0.5% to 0.7% (according to the PGDL report). At the discharge site, the tunnel has a width of 38.8m and a height of 2.5m, and the bottom of the tunnel's mouth lies at a depth of 1.56m. The tunnel is predicted to be able to handle runoff in excess of 160 m³/s. A figure of the general outline of the tunnel is shown in Figure 4, while the technical drawing is presented as an annex.

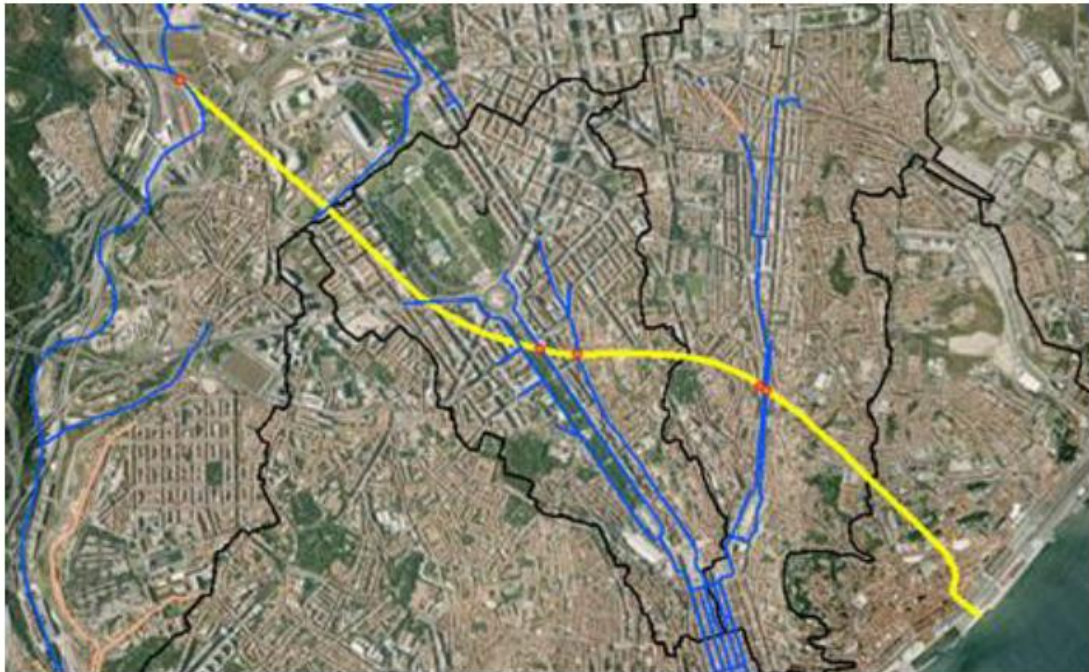


Figure 4 - General outline of the discharge tunnel, in yellow. (PGDL, 2015)

Additionally, in order to minimise the extent of the first flush effect (wherein the concentration of pollutants is very high within the discharged water), the initial runoff will be diverted to the Alcântara WWTP (PGDL, 2015). In accordance to this WWTP's treatment capacity, the flow diverted is up to 6.6m³/s.

3. Methodology

3.1 The Mathematical Model

The computer modelling software MOHID water was used in this study (www.mohid.com). MOHID is a three-dimensional water modelling system, developed by MARETEC (Marine and Environmental Technology Research Center) at IST (Instituto Superior Técnico), which is a part of ULisboa (Universidade de Lisboa, University of Lisbon). The philosophy behind MOHID is object-oriented programming, meaning that MOHID offers good integrating tools for processes (physical, biological, chemical, geological), hydrological systems (estuaries and watersheds) as well as for different scales. This last item is particularly relevant for this thesis, as it allowed the creation of a nested model. MOHID has been applied in numerous modelling studies, attesting to its robustness and reliability.

MOHID has been used extensively to model hydrodynamic phenomena, especially with regards to estuarine and coastal water bodies. For example, Pierini et al. (2008) used it to model the evolution of two properties, namely salinity and temperature, in Bahía Blanca estuary in Argentina, whereas Campuzano (2008) vertically modelled the Aysén fjord not only in terms of salinity and temperature, but also in terms of velocity vectors. Specifically of interest to this work is the fact that MOHID is used in numerous studies of the Tagus estuary, such as Pinto et al. (2013) which is a complex work that aims to couple DEB theory to MOHID and use it to study a number biogeochemical processes in addition to physical ones, and how they relate to mussel growth, and Mateus and Oliveira (2013) simulates CO₂ dynamics as well as a number of other elements, such as nitrogen and phosphorus.

Throughout the years, for both hydrodynamic and biogeochemical processes in the Tagus estuary, the model has been continuously validated and calibrated via monitoring data. MOHID's modelling data and parametrization as it relates to the Tagus estuary is continuously calibrated and curated by MARETEC, and is therefore considered an accurate source of such data.

The hydrodynamic module solves the three-dimensional incompressible primitive equations, assuming hydrostatic equilibrium and Boussinesq and Reynolds approximations. The momentum balance equations for mean flow horizontal velocities in Cartesian form are:

$$\frac{\partial u}{\partial t} = -\frac{\partial(uu)}{\partial x} - \frac{\partial(uv)}{\partial y} - \frac{\partial(uz)}{\partial z} + fv - \frac{1}{\rho_0} \frac{\partial p}{\partial y} + \frac{\partial((v_H) \frac{\partial u}{\partial x})}{\partial x} + \frac{\partial((v_H) \frac{\partial u}{\partial y})}{\partial y} + \frac{\partial((v_V) \frac{\partial u}{\partial z})}{\partial z} \quad (\text{Eq. 1})$$

$$\frac{\partial v}{\partial t} = -\frac{\partial(vu)}{\partial x} - \frac{\partial(vv)}{\partial y} - \frac{\partial(vz)}{\partial z} - fu - \frac{1}{\rho_0} \frac{\partial p}{\partial x} + \frac{\partial((v_H) \frac{\partial v}{\partial x})}{\partial x} + \frac{\partial((v_H) \frac{\partial v}{\partial y})}{\partial y} + \frac{\partial((v_V) \frac{\partial v}{\partial z})}{\partial z} \quad (\text{Eq. 2})$$

where u , v and w are the components of the velocity vector in the x , y and z directions respectively, f is the Coriolis parameter, ν_H and ν_V are the turbulent viscosities in the horizontal and vertical directions respectively and p is the pressure.

The vertical velocity is calculated from the incompressible continuity equation (mass balance equation):

$$\frac{\partial u}{\partial x} + \frac{\partial v}{\partial y} + \frac{\partial w}{\partial z} = 0 \quad (\text{Eq. 3})$$

The free surface equation is achieved as a result of the integration of the equation of continuity over the whole water column (between the free surface elevation $z=\eta(x,y,t)$ and the bottom $z=-h(x,y)$):

$$\frac{\partial \eta}{\partial t} = -\frac{\partial \int_{-h}^{\eta} u dz}{\partial x} - \frac{\partial \int_{-h}^{\eta} v dz}{\partial y} \quad (\text{Eq. 4})$$

The equation for hydrostatic pressure is

$$\frac{\partial p}{\partial z} + g\rho = 0 \quad (\text{Eq. 5})$$

where g is gravity and ρ is density. Vertically integrating this equation, defining p_{atm} to be atmospheric pressure, ρ_0 to be a constant reference density and ρ' to be a deviation from that constant reference density, and considering $\rho = \rho_0 + \rho'$, yields:

$$p(z) = p_{atm} + g\rho_0(\eta - z) + g \int_z^{\eta} \rho' dz \quad (\text{Eq. 6})$$

This equation relates pressure at any depth with the atmospheric pressure at the sea surface, the sea level and the anomalous pressure integrated between that level and the surface. By using this expression and the Boussinesq approximation, the horizontal pressure gradient in the direction x_i can be divided in three contributions:

$$\frac{\partial p}{\partial x_i} = \frac{\partial p_{atm}}{\partial x_i} - g\rho_0 \frac{\partial \eta}{\partial x_i} - g \int_z^{\eta} \frac{\partial \rho'}{\partial x_i} dz \quad (\text{Eq. 7})$$

In terms of the water properties module, it coordinates the evolution of the water properties in the water column, using an eulerian approach. This coordination includes the transport due to advective and diffusive fluxes, water discharges from rivers or anthropogenic sources, exchanges with the bottom

(sediment fluxes) and the surface (heat fluxes and oxygen fluxes), sedimentation of particulated matter and the internal sinks and sources (water quality). The transport due to advective and diffusive fluxes of a given property A, is resolved by the following equation:

$$\frac{\partial A}{\partial t} = -\frac{\partial(uA)}{\partial x} - \frac{\partial(vA)}{\partial y} - \frac{\partial(wA)}{\partial z} + \frac{\partial(k_H \frac{\partial A}{\partial x})}{\partial x} + \frac{\partial(k_H \frac{\partial A}{\partial y})}{\partial y} + \frac{\partial(k_V \frac{\partial A}{\partial z})}{\partial z} + (S_0 - S_i) \quad \text{(Eq. 8)}$$

where k_H and k_V are the horizontal and vertical turbulent diffusivities of the property, and $(S_0 - S_i)$ represents the sources minus the sinks.

The density is computed as a function of temperature and salinity by the UNESCO density equation (Fofonoff and Millard, 1983).

As for the sediments module, it “aims to simulate the dynamics of sediments found in natural systems” (Franz et al., 2017). The basic conceptual model uses four layers. The water layer is the water column, where sediments are carried suspended in the water via advection and diffusion. The fluid mud layer is a layer which may or may not form, based on the presence or lack of mud and the kinetic conditions of the water body. The active layer is the upper layer of the bottom which is in contact with the water column, and is affected by currents and waves; it may become part of the settled layer in case of net aggradation, with a new active layer being formed above it. The settled layer is the sediments’ stratigraphy, and the top of this layer may become the new active layer in case of net scour. This model and the way each layer interacts with each other is illustrated in Figure 5.

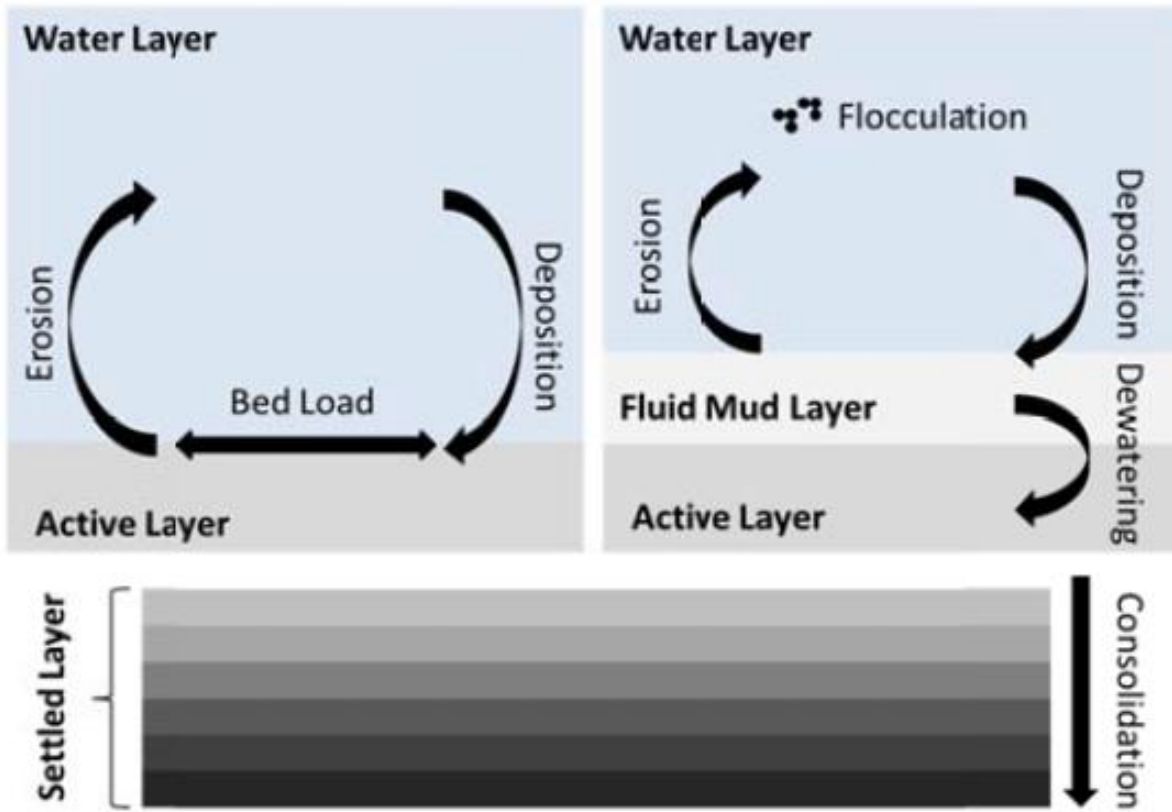


Figure 5 - Sediment module's model layers and associated processes. The different shades in the settled layer represents sediment stratigraphy. (Franz et al. 2017)

The water layer has, within itself, suspended sediment transport handled by the three-dimensional advection-diffusion equation (Eq. 8), treating mud (cohesive sediment) and sand as water properties. The water layer trades mud with the fluid mud layer by mud erosion and flocculated mud deposition. This layer also trades sand with the active layer, via sand erosion and deposition. It is possible that mud is traded directly between the active and water layers if the fluid mud layer does not form.

The active layer may take mud from the fluid mud layer in case of mud deposition. There is also bedload transport of sand along the active layer, which involves horizontal transport of non-cohesive sediment by gliding, rolling or saltating sand particles.

The settled layer may be subject to consolidation, approximated by an increase in dry density of the cohesive sediments in this layer. As a result of erosive and depositional processes, the bed evolution is computed, resulting in bathymetric changes.

3.2 Model setup

In order to study two levels of spatial detail, two models were developed for both the hydrodynamic and morphodynamic studies: the "main" model and the "nested" model. The "nested" model is nested

on the "main" model and uses it as boundary conditions. The "main" model uses larger grid cells and time steps and refers to a larger area, whereas the "nested" model goes over more minute details and has more precise computations (given the smaller time step for each calculation). Descriptions for the two models are detailed below.

3.2.1 Location

The boundaries of the geographic area of the "main" model implementation are roughly from Cais do Sodré to Xabregas along Lisbon's coast, and then up to 1.15 to 1.6 km away from the coast. The approximate location is displayed in Figure 6.



Figure 6 - Approximate location of the "main" model's geographical extent.

As for the "nested" model, it is approximately located in the area from Santa Apolónia's train station to the fado museum along the coast, and then approximately 300m away from the coast, as shown in Figure 7.



Figure 7 - Approximate location of the "nested" model's geographical extent.

The coordinates for both domains are displayed in Table 1.

Table 1 - Coordinates of "main" and "nested" models' domains.

	Northernmost coordinates	Easternmost coordinates	Southernmost coordinates	Westernmost coordinates
"main" model	38.7249 N, 9.1079 W	38.7117 N, 9.1003 W	38.6892 N, 9.1393 W	38.7031 N, 9.1473 W
"nested" model	38.7133 N, 9.1218 W	38.7108 N, 9.1203 W	38.7075 N, 9.1262 W	38.7094 N, 9.1272 W

3.2.2 Bathymetry

Over the described areas, a grid was laid out. This grid's resolution is 25x25m² for the "main" model, and in order to better suit the location under study, a 30° rotation was applied. The grid itself is 180 cells long and 64 cells wide, as shown in Figure 8.

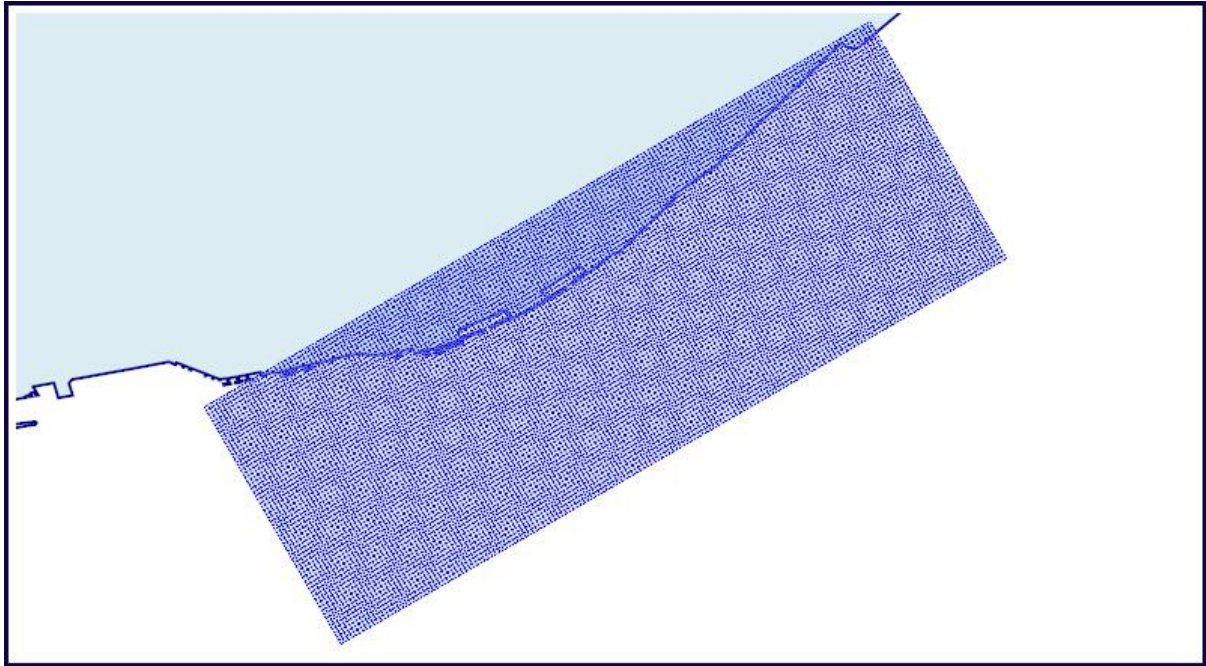


Figure 8 - "main" model grid over Lisbon's coastline.

As for the "nested" model, the resolution of the grid is $5 \times 5 \text{m}^2$ and it has the same 30° rotation. The grid is 135 cells long and 60 cells wide, as illustrated in Figure 9.

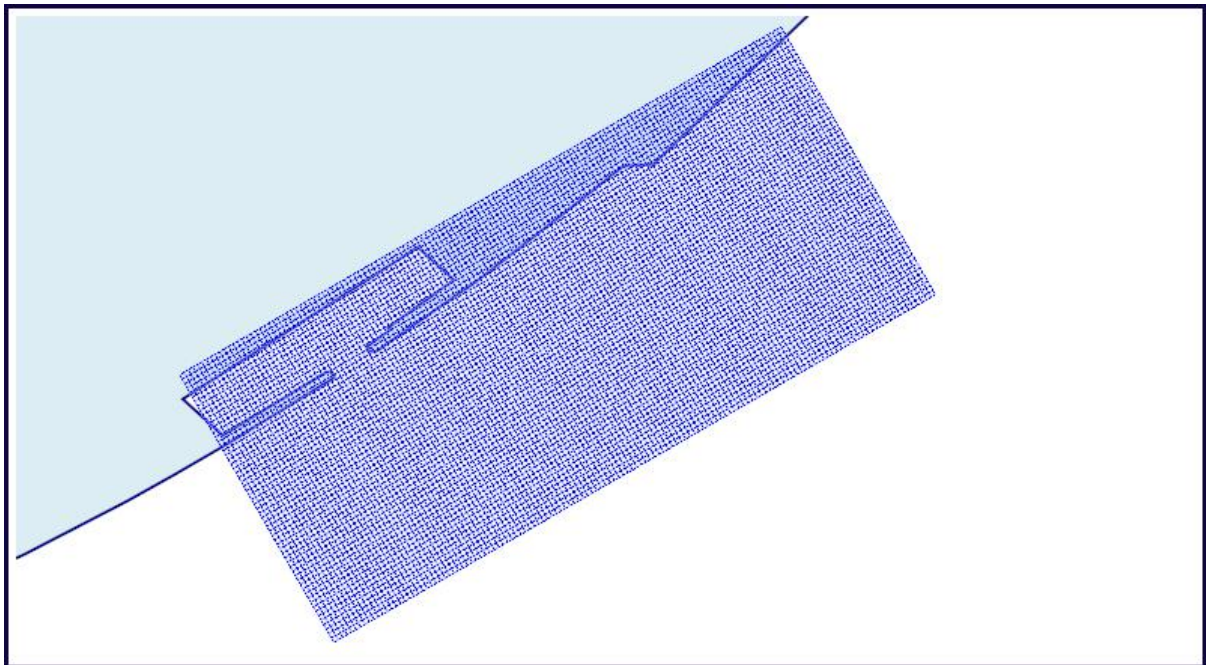


Figure 9 - "nested" model grid over Lisbon's coastline.

Afterwards, two bathymetry files were created using these grids, the definition of Lisbon's coastline (via a file supplied by MARETEC) and the bathymetric points on the Tagus estuary (also supplied by MARETEC), by interpolating the bathymetric information into the grids, with the resulting bathymetric files shown below, in Figures 10 and 11.

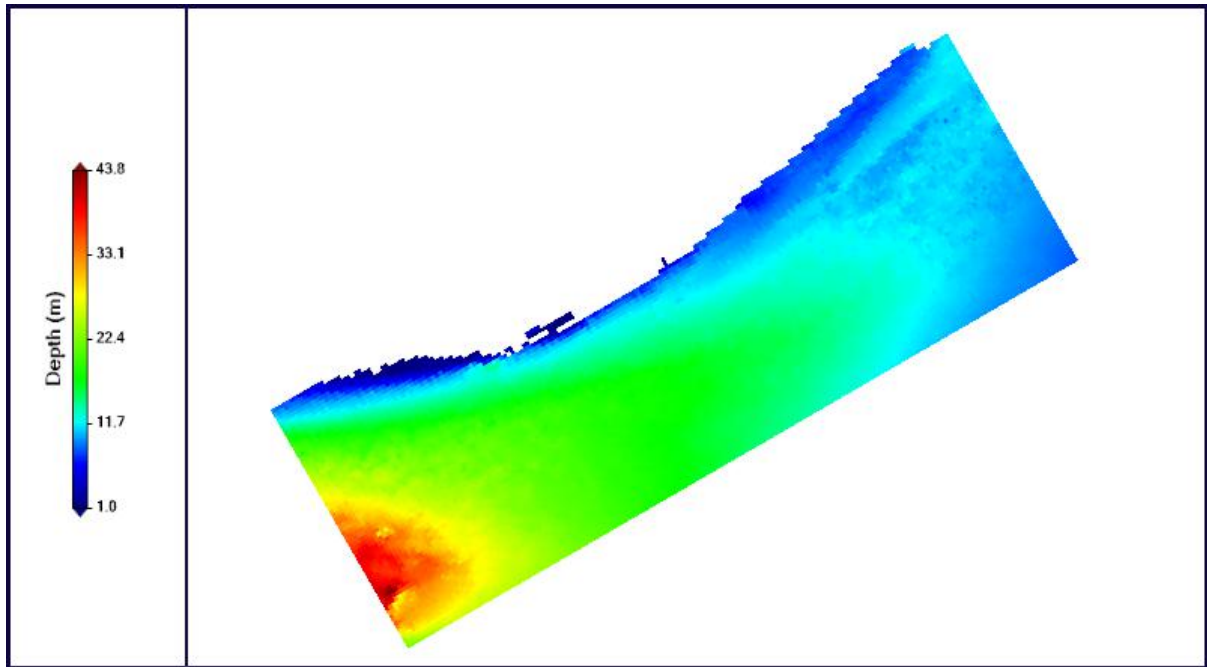


Figure 10 - "main" model bathymetry.

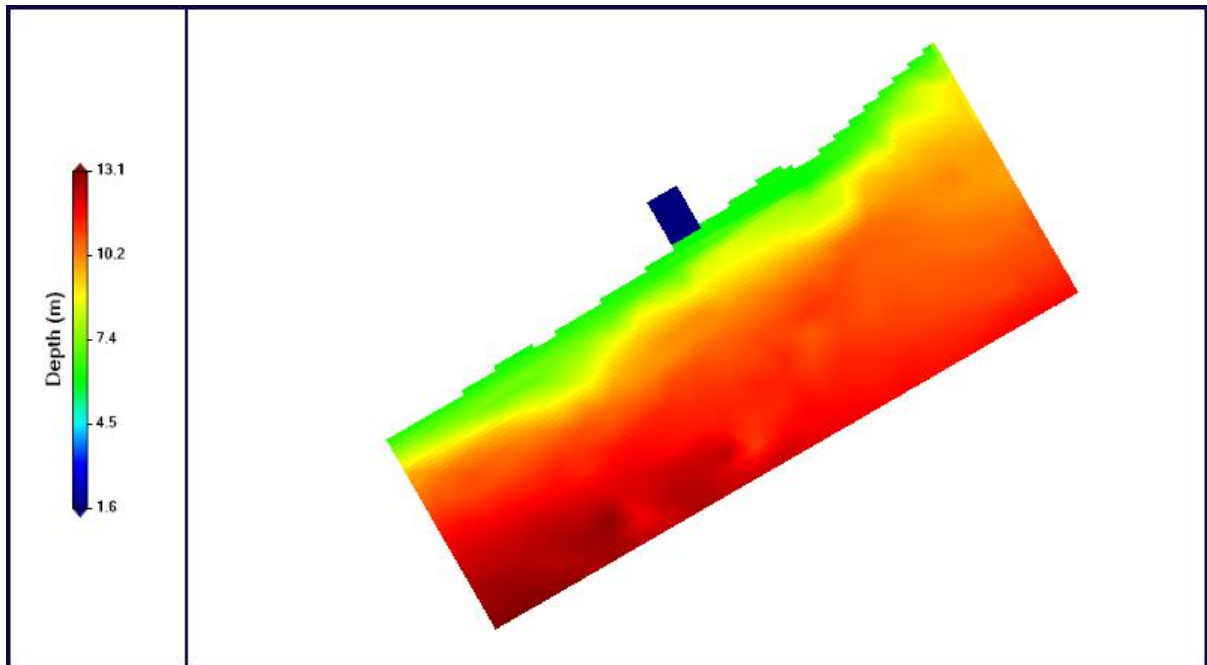


Figure 11 - "nested" model bathymetry.

3.2.3 Model parametrization

The models were set to simulate a 12-hour period with a computational time step of 1.5 seconds for the "main" model and 0.25 seconds for the "nested" model.

The simulated discharge was set to 160m³/s as previously stated, and the discharged load was defined as being water with a generic property set to 1 000 000 (arbitrary units), no sediments, and no other properties. The discharge was set to begin immediately after the first hour of the run (meaning, the model runs the first hour without any discharge) and set to stop at eleven hours after the run begun. The discharge was set to occur at the coordinates 9.1243 W, 38.7116 N, in the cell with grid coordinates I=48, J=97 of the "main" model. In the "nested" model, the discharge occurs in the line defined between the points with grid coordinates I=59, J=70 and I=59, J=76.

The locations for the time series were chosen based on dispersion in the domain, meaning that the methodology adopted for selection the locations was to set one location to each corner of the model and one to the midway point between those locations, then one at the mouth of the discharge tunnel, and one at the centre of the domain. The locations for the time series are shown on Figures 12 and 13, and their exact coordinates are detailed in Table 2.

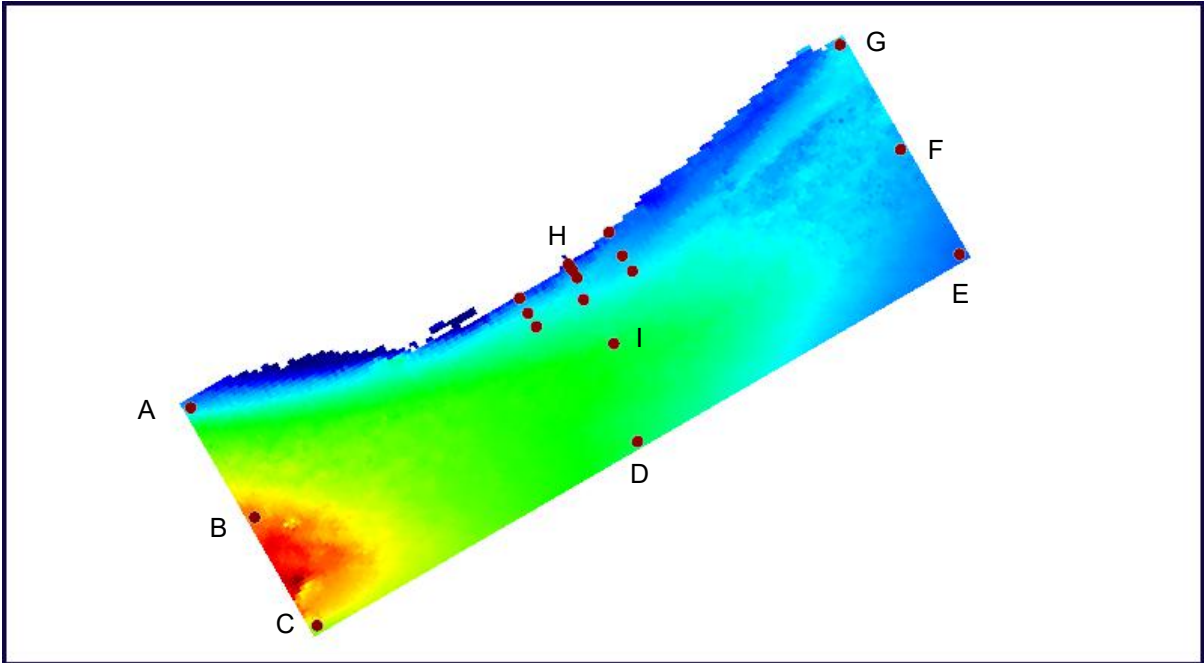


Figure 12 - Locations for the time series for the "main" model, in dark red.

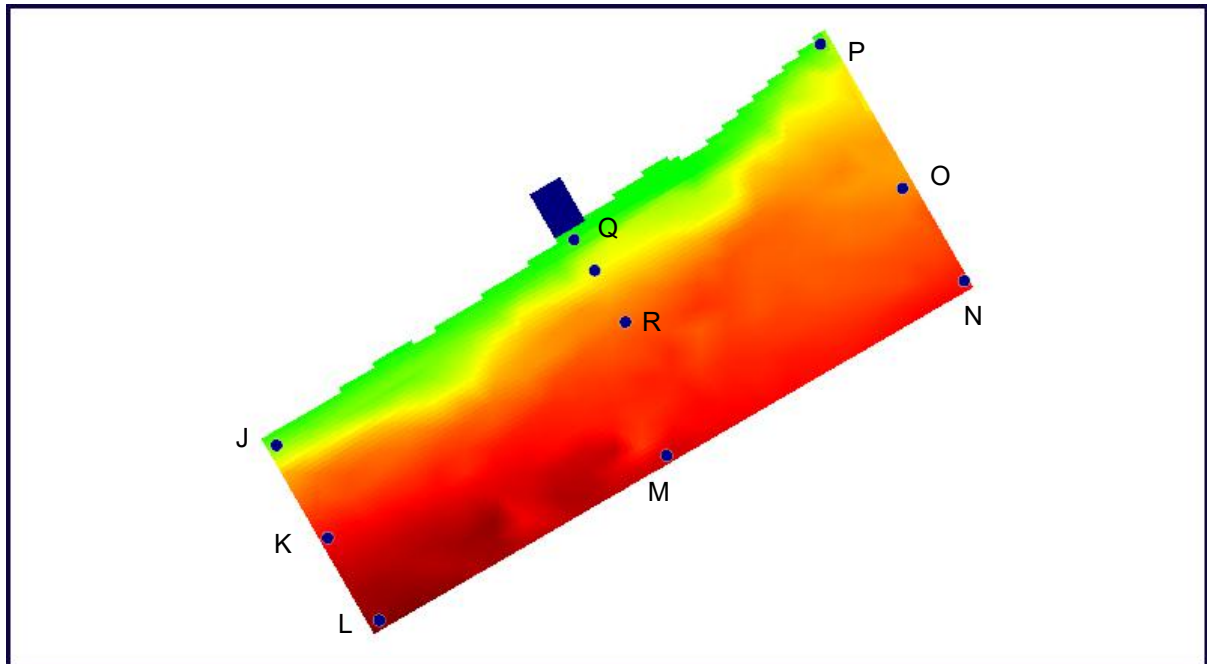


Figure 13 - Locations for the time series for the "nested" model, in dark blue.

Table 2 - ID, locations and coordinates for the time series' locations.

ID	Location	Latitude	Longitude
A	Top-left of "main" model	38.7028 N	9.1466 W
B	Centre-left of "main" model	38.6963 N	9.1428 W
C	Bottom-left of "main" model	38.6899 N	9.1391 W
D	Centre-bottom of "main" model	38.7008 N	9.1201 W
E	Bottom-right of "main" model	38.7119 N	9.1010 W
F	Centre-right of "main" model	38.7181 N	9.1045 W
G	Top-right of "main" model	38.7243 N	9.1081 W
H	Mouth of the discharge tunnel - "main" model	38.7110 N	9.1240 W
I	Centre of the domain - "main" model	38.7066 N	9.1215 W
J	Top-left of "nested" model	38.7093 N	9.1271 W
K	Centre-left of "nested" model	38.7084 N	9.1266 W
L	Bottom-left of "nested" model	38.7076 N	9.1261 W
M	Centre-bottom of "nested" model	38.7092 N	9.1233 W
N	Bottom-right of "nested" model	38.7109 N	9.1204 W
O	Centre-right of "nested" model	38.7118 N	9.1210 W
P	Top-right of "nested" model	38.7132 N	9.1218 W
Q	Mouth of the discharge tunnel - "nested" model	38.7113 N	9.1242 W
R	Centre of the domain - "nested" model	38.7105 N	9.1237 W

The model assimilates boundary conditions in its open boundaries (i.e. non-land boundaries), as well as tide and general hydrodynamic conditions (water level and velocity) from a previous simulation of the entire Tagus estuary. This way, the border conditions are set according to this previous simulation of the Tagus estuary, in which there is no discharge tunnel, and therefore reflect the estuary “as is”, in its current state.

The modelled domain is divided vertically in two subdomains, both with σ (sigma) coordinates. Sigma coordinates adapt to bathymetry and change in accordance to the water column. Thicknesses are defined as a percentage of the water column. The first domain has 10 layers, each with 10% of the total subdomain height, and is the domain adjacent to the bottom. The second domain has 5 layers, each measuring 20% of the total subdomain height, and is located above the other domain, that is, adjacent to the surface. This was done so that the compensation due to rising or falling water level (because of the tide) would affect only the top domain. At the water-sediment interface, only the shear stress was computed. The rugosity was set to 0.0025. The output times for all desired results were set at 10 minutes.

For the hydrodynamics and water properties, the computed variables were the water level, velocity, and a generic property. For the sediment module, the desired results were those regarding different sand classes, cohesive sediments, and bathymetry evolution.

The water column was set as having no sand, but 30 mg/L of cohesive sediments, uniformly distributed along the water column. The sediment column or settled layer was defined as having no cohesive sediment, but having sand. The sand classes were defined as shown in Table 3:

Table 3 - Sand classes, with d_{50} being the median diameter of each class, considered to be the representative diameter of each class.

Class	d_{50} (mm)	ID
1	0.2	Very fine
2	0.6	Fine
3	1	Medium
4	1.4	Coarse
5	1.8	Very coarse

The sediment column was defined, for the whole domain, as being 2m in height. It was divided into 20 layers - the top 15 were set as empty (to be filled, in case of net aggradation) and the bottom 5 were considered to each be filled with a single sand class. Each layer was considered to have equal height to one another (considering the 2m height of the sediment column, that means each of the 5 filled layers tally 20% of the total height, or 0.4m each). This means that the top layer is 0.4m of exclusively very fine (class 1) sand, the second layer is 0.4m of exclusively fine (class 2) sand, and so on. Actual sediment distribution in the Tagus river’s estuary was not used, as such data was not found, and as such this distribution must be considered a schematic or case study, and the results cannot be interpreted strictly as the real sediment distribution.

3.3 Results' analysis

The distances in the results section were calculated according to:

$$d = (\sqrt{(x_i - x_f)^2 + (y_i - y_f)^2}) \times r \quad \text{(Eq. 10)}$$

where: d is the distance (m); x_i is the first coordinate of the discharge location; x_f is the first coordinate of the furthest location in which the concentration of the generic property is at least the desired percentage of the initial concentration; y_i is the second coordinate of the discharge location; y_f is the second coordinate of the furthest location in which the concentration of the generic property is at least the desired percentage of the initial concentration; and r is the distance between the centre of two adjacent cells.

4. Results

In this chapter, in all the vertically cut images presented, the ones pertaining to the "main" model have a vertical distortion coefficient of 50 (Figures 15, 17, 19, 21, 23, 25, 27, 36, 38 and 40); as for the ones regarding the "nested" model, this distortion coefficient is 15 (Figures 45, 46, 53, 54 and 55). All the vertical cut images are cut at the centre of the discharge tunnel; this means, for the "main" model, the cells shown are from (1,97) to (49,97), or (38.7014 N, 9.1185 W) to (38.7118 N, 9.1245 W); for the "nested" model, they are from (1,73) to (59,73), or (38.7093 N, 9.1230 W) to (38.7118 N, to 9.1245 W).

4.1 Hydrodynamics

In this section, the results for the water level (as it relates to tidal circulation), the velocity field, and water properties are presented.

4.1.1 Velocity modulus, velocity field and water level

Here, the evolution of the velocity modulus and current direction throughout the 12 hour simulated period are described and displayed.

For the "main" model, at the initial instant, during the flood tide, the current is coming into the estuary. The discharge hasn't yet begun at this point, and as such the only hydrodynamic forces affecting the velocity field and modulus is the tide, which is noticeable in the resulting horizontal map image (Figure 14) as well as in the vertical cut image (Figure 15).

At the 01:10:00 instant (Figures 16 and 17), at the tidal maximum (high tide), the discharge begins. At this point the water level is at its peak, and the average velocity modulus at its minimum. The maximum velocity at this instant is observed at the tunnel's discharge location, which was expected, since at this instant the most relevant impact on the model is the discharge, since the tide has reached its peak height and as such the tidal component of the velocity modulus is minimal.

At the 03:30:00 instant, during the ebb tide, the maximum average velocity is achieved and the effect of both the discharge and the tide are observable. There is a wedge in the velocity field wherein the interaction between the tide and the discharge, perpendicular to the flow, is noticeable from the horizontal map image (Figure 18). It is interesting to note that in the vertical cut image (Figure 19) the vertical effect of this wedge is noticeable, and seems to be spreading outwards from the coast.

At the 07:00:00 instant (Figure 20), the water level is at its lowest point (low tide). The effect of the tunnel's discharge is noticeable, as it is once again the main hydrodynamic force actuating in the

model at this time. The area affected has an approximate radius of 1150m. In the vertical cut image (Figure 21), it is clear that the tunnel discharge's effect is only affecting the surface, having very little impact even a few meters below the water surface.

At the 10:10:00 instant, during flood tide, the symmetrical situation to that of 03:30:00 is observed; meaning, the flood tide is causing the water level to increase and the velocity modulus is again at its maximum, albeit in the contrary direction to that of 03:30:00. The wedge-like effect of the tunnel's discharge on the tide is more noticeable than before in the horizontal map image (Figure 22), and there is again a noticeable vertical effect, seen in the vertical cut image (Figure 23). This is the first instant after the end of the discharge.

At 11:10:00 (Figure 24), one hour after the end of the discharge, its effects are almost negligible on the estuary. The vertical cut (Figure 25) show no signs of the effects of the discharge, and the only noticeable effect seems to be a vestigial wedge where it was at 10:10:00.

At the final instant, 12:00:00 (Figures 26 and 27), the situation is similar to the initial instant. Once again at flood tide, and once again the only hydrodynamic force impacting the estuary being the tide - in other words, the effect of the discharge is not felt.

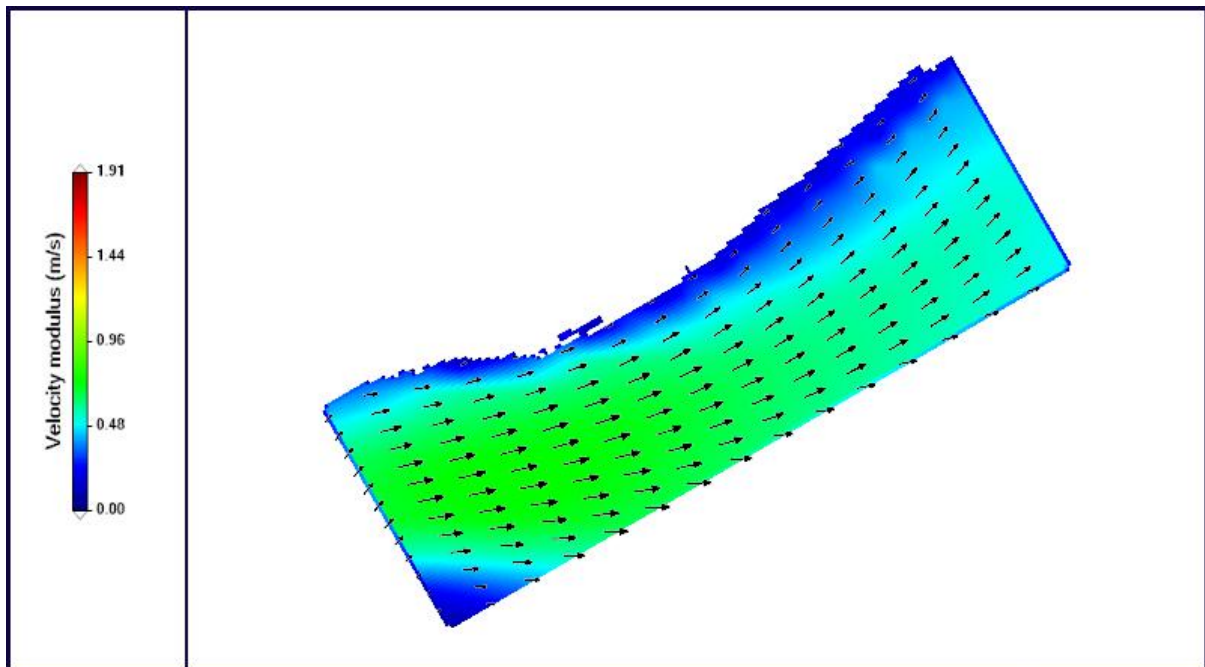


Figure 14 - Velocity modulus (m/s) and field at 00:00:00, "main" model, horizontal map image.

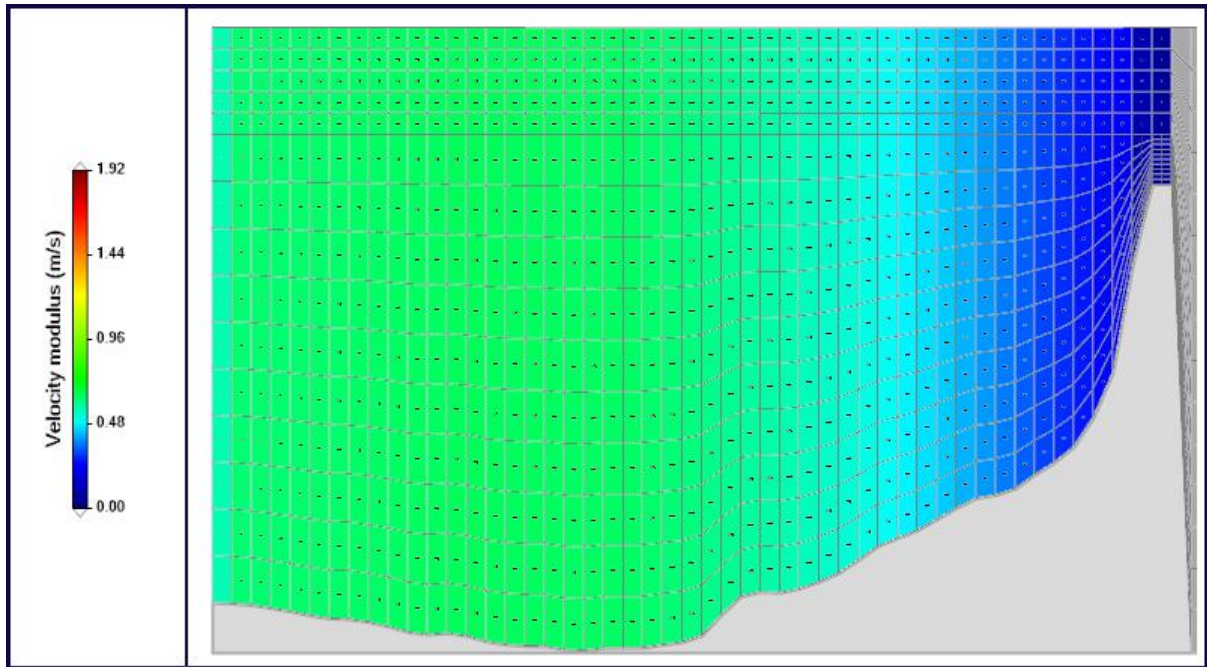


Figure 15 - Velocity modulus (m/s) and field at 00:00:00, "main" model, vertical cut image.

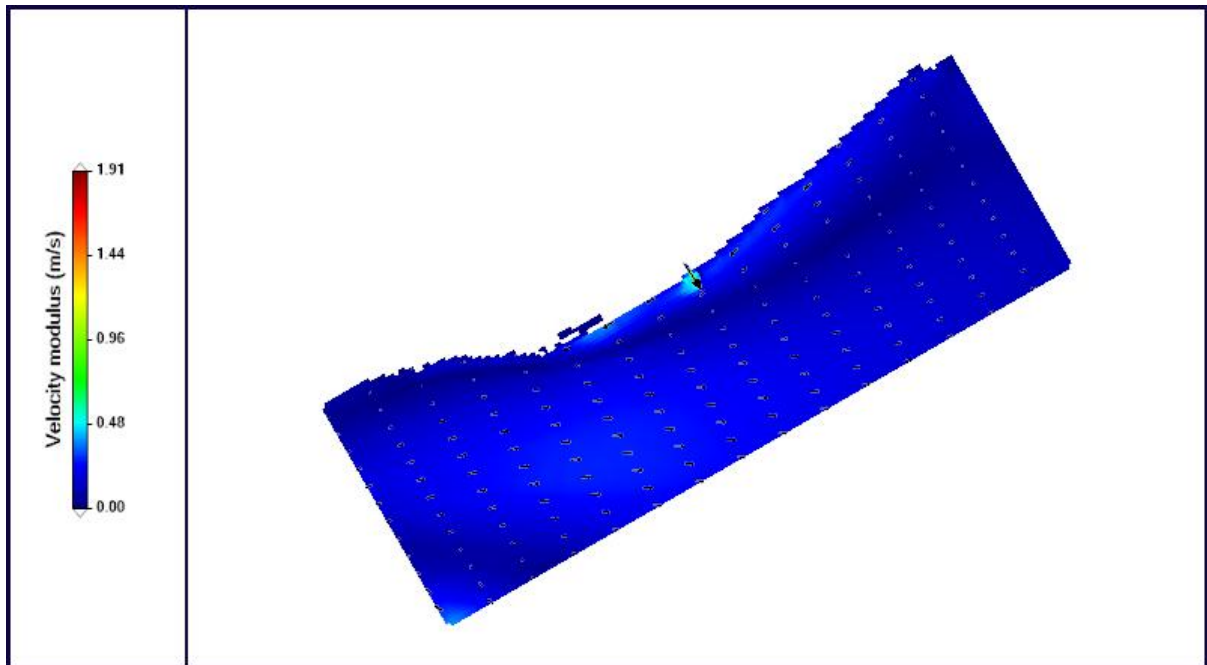


Figure 16 - Velocity modulus (m/s) and field at 01:10:00, "main" model, horizontal map image.

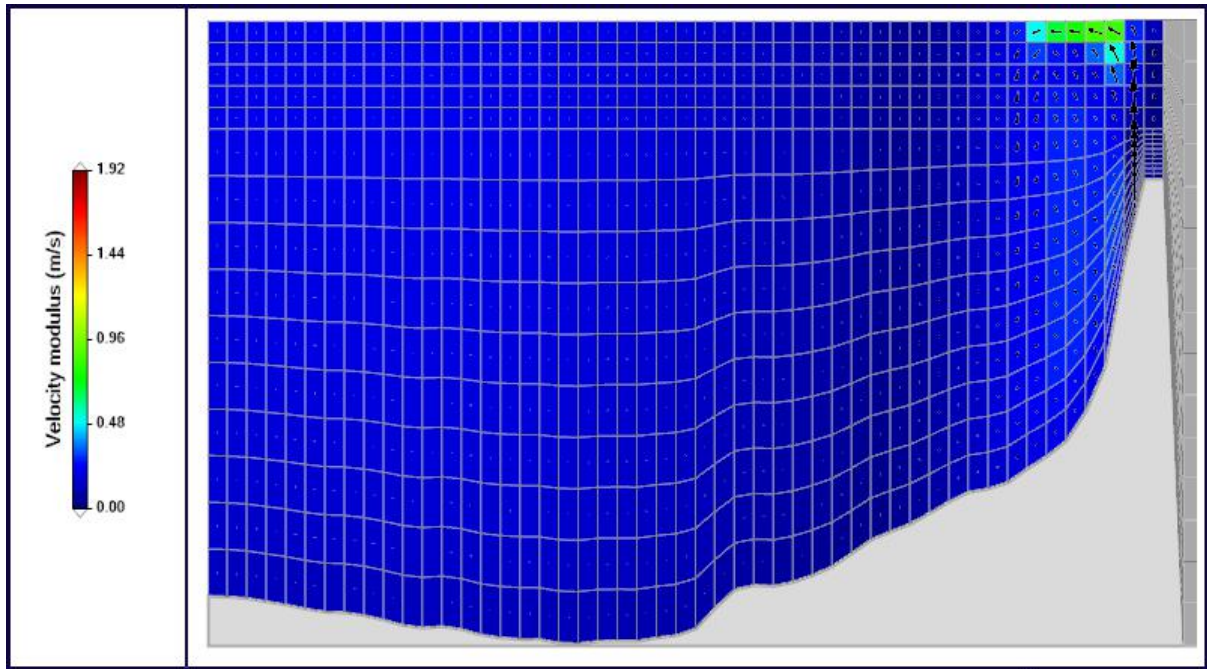


Figure 17 - Velocity modulus (m/s) and field at 01:10:00, "main" model, vertical cut image.

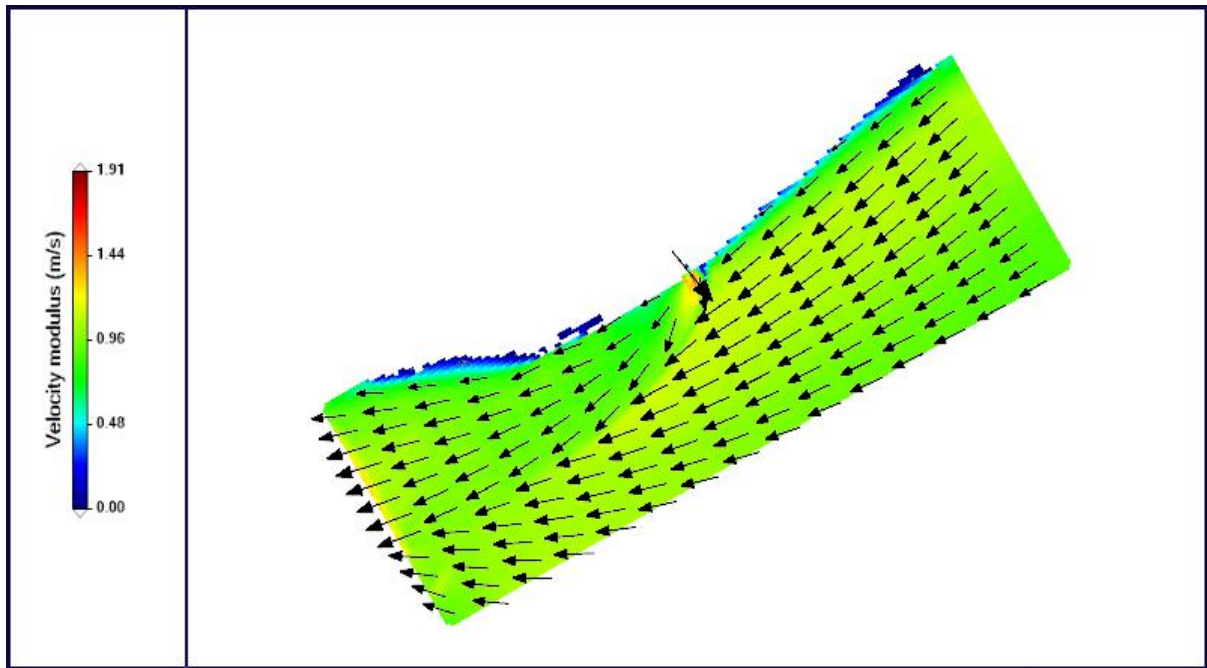


Figure 18 - Velocity modulus (m/s) and field at 03:30:00, "main" model, horizontal map image.

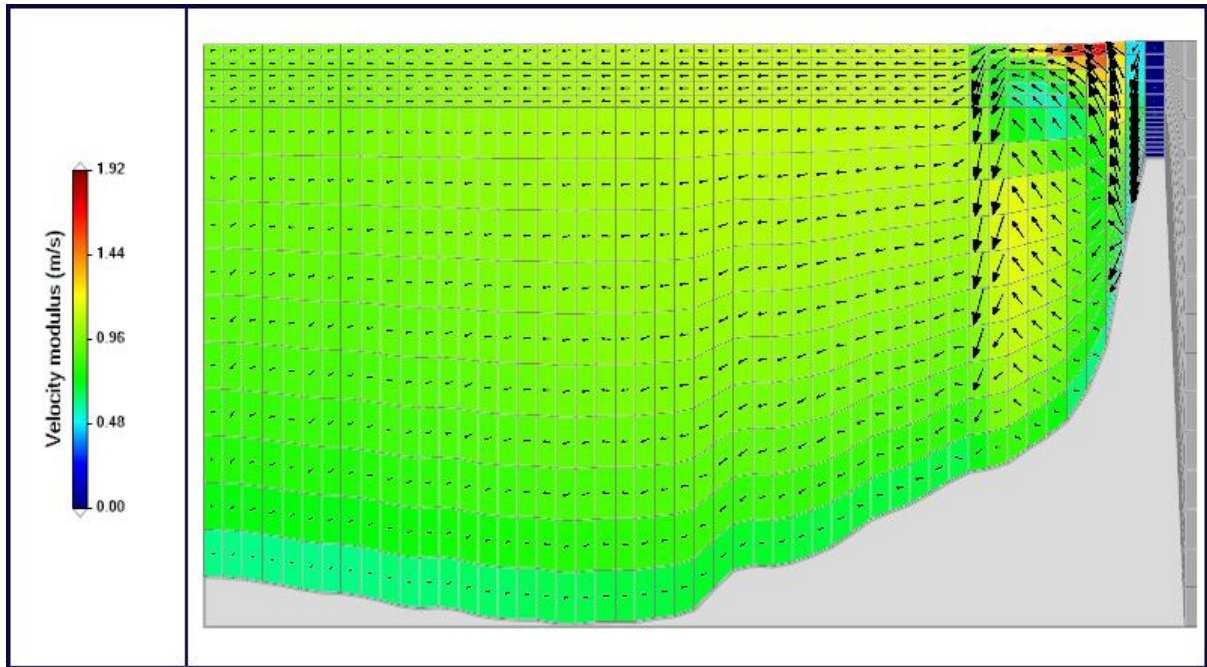


Figure 19 - Velocity modulus (m/s) and field at 03:30:00, "main" model, vertical cut image.

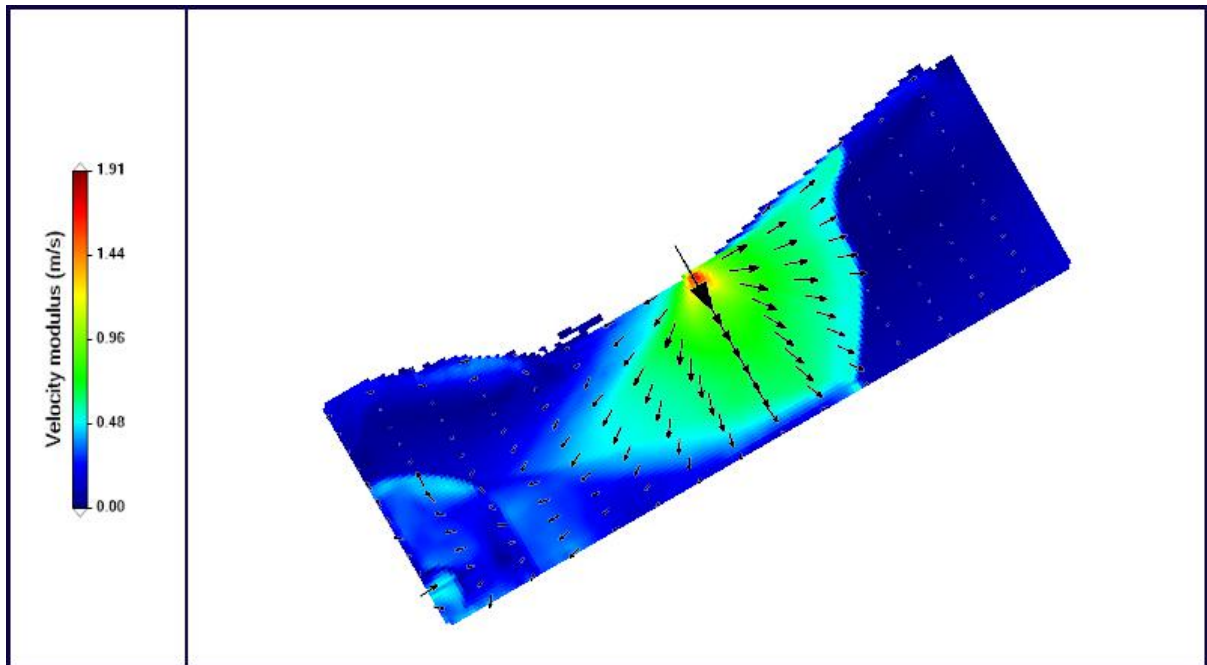


Figure 20 - Velocity modulus (m/s) and field at 07:00:00, "main" model, horizontal map image.

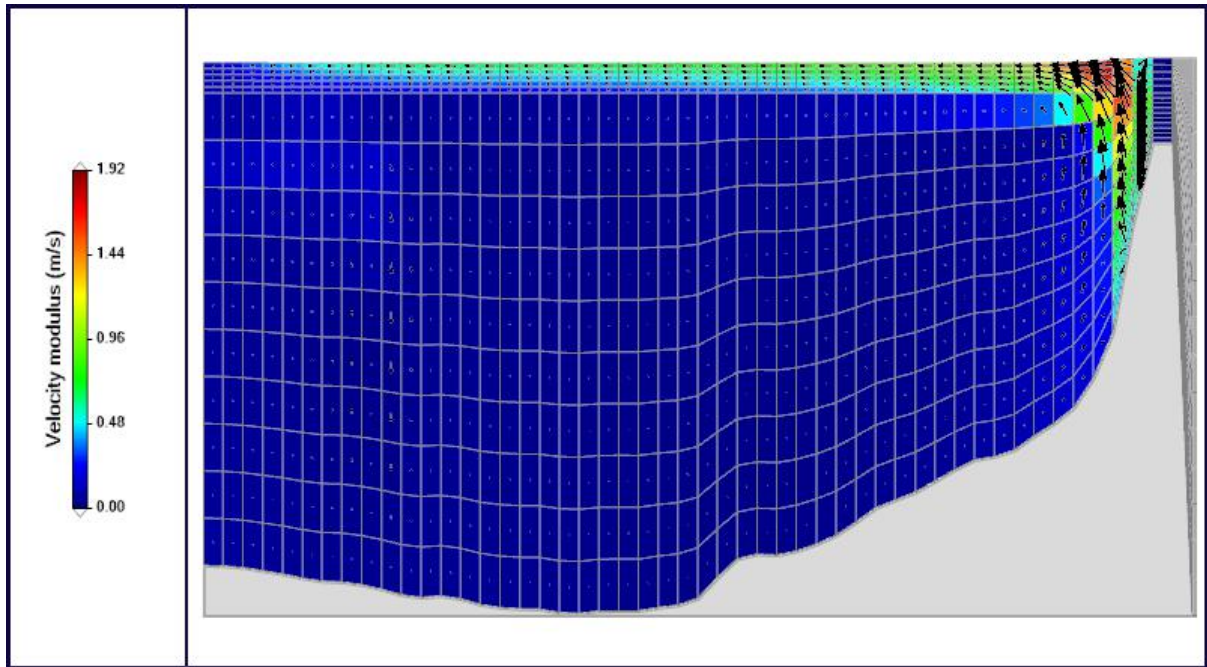


Figure 21 - Velocity modulus (m/s) and field at 07:00:00, "main" model, vertical cut image.

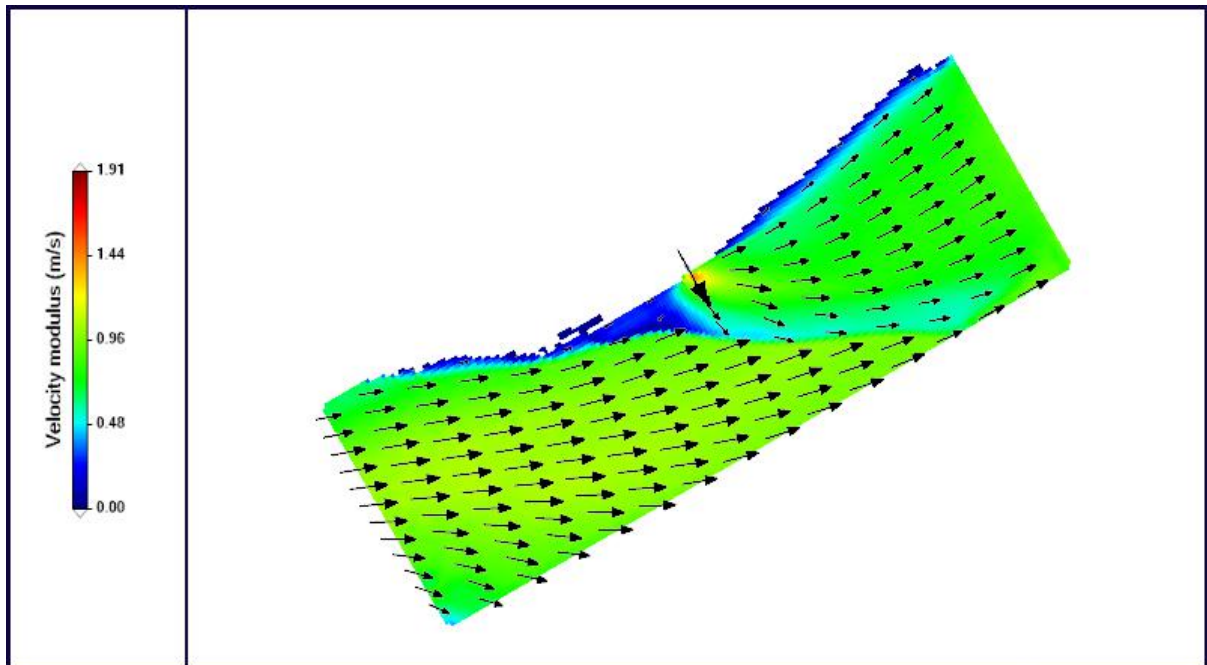


Figure 22 - Velocity modulus (m/s) and field at 10:10:00, "main" model, horizontal map image.

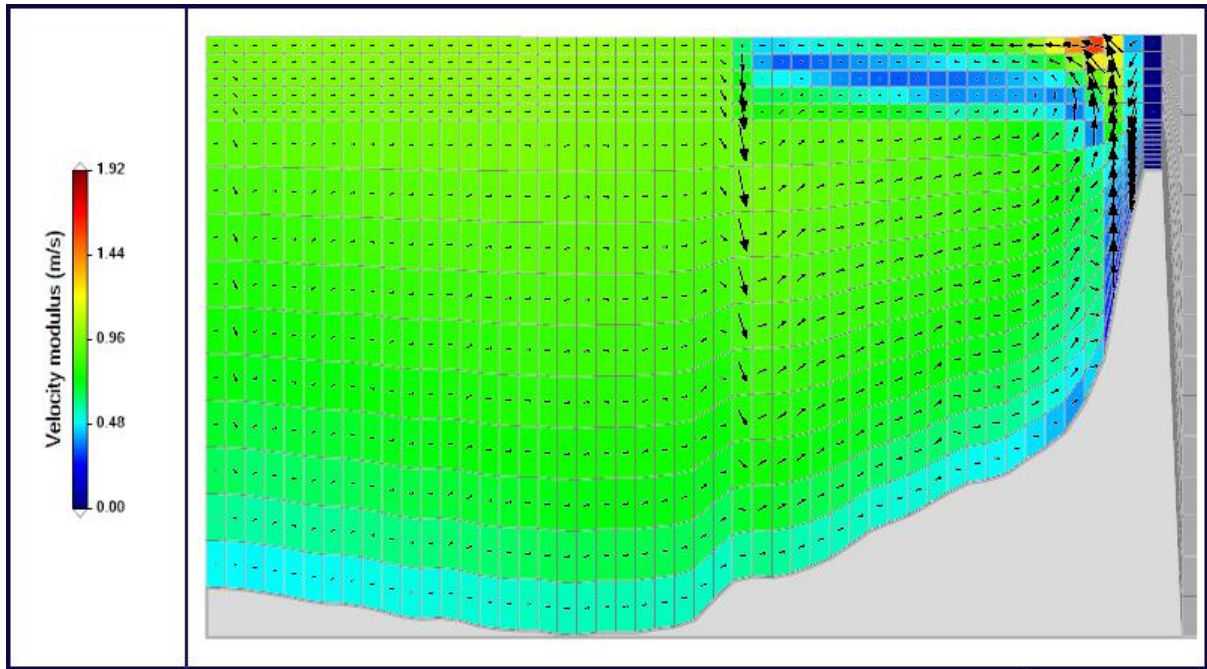


Figure 23 - Velocity modulus (m/s) and field at 10:10:00, "main" model, vertical cut image.

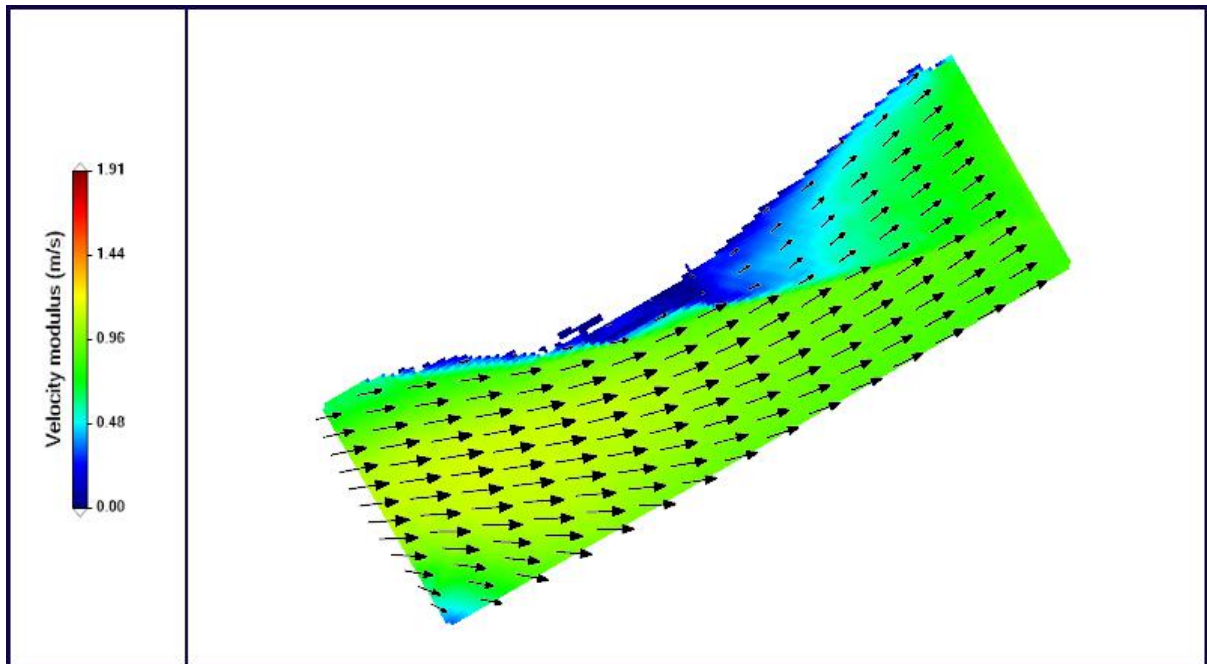


Figure 24 - Velocity modulus (m/s) and field at 11:10:00, "main" model, horizontal map image.

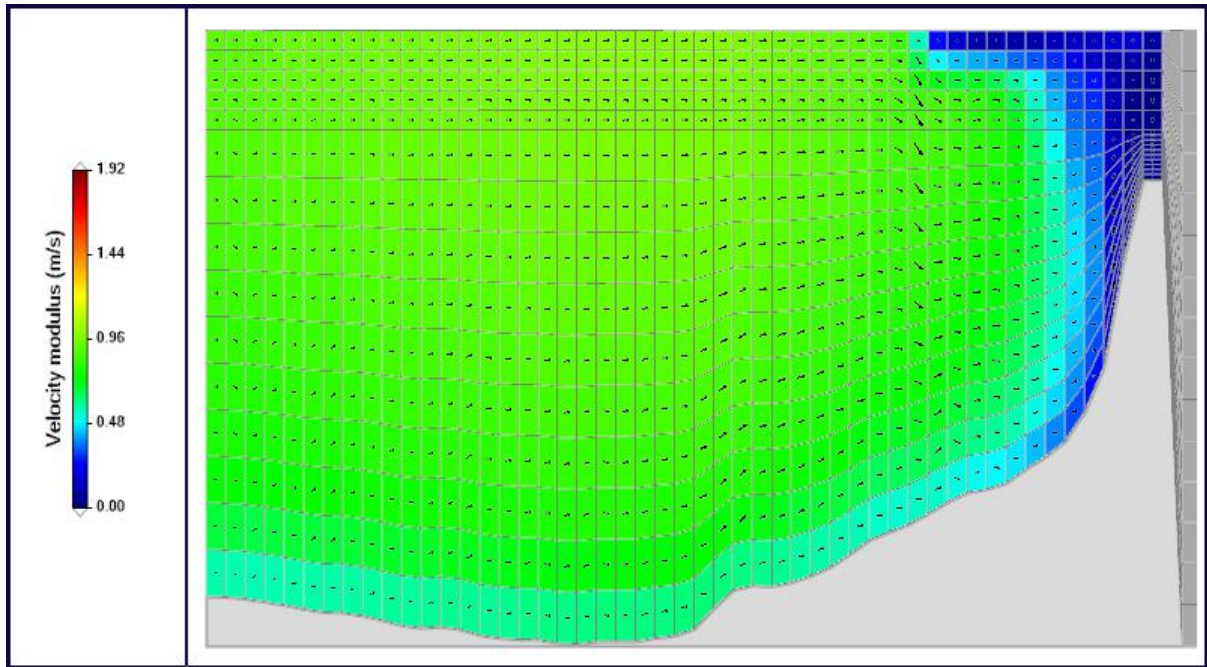


Figure 25 - Velocity modulus (m/s) and field at 11:10:00, "main" model, vertical cut image.

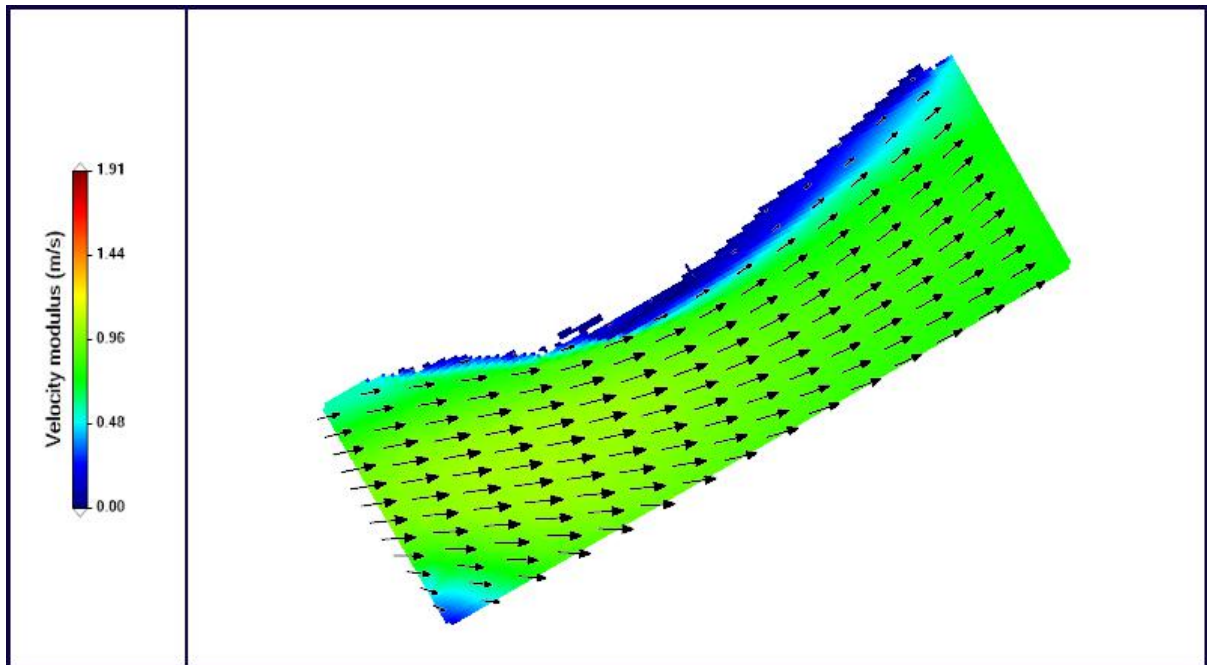


Figure 26 - Velocity modulus (m/s) and field at 12:00:00, "main" model, horizontal map image.

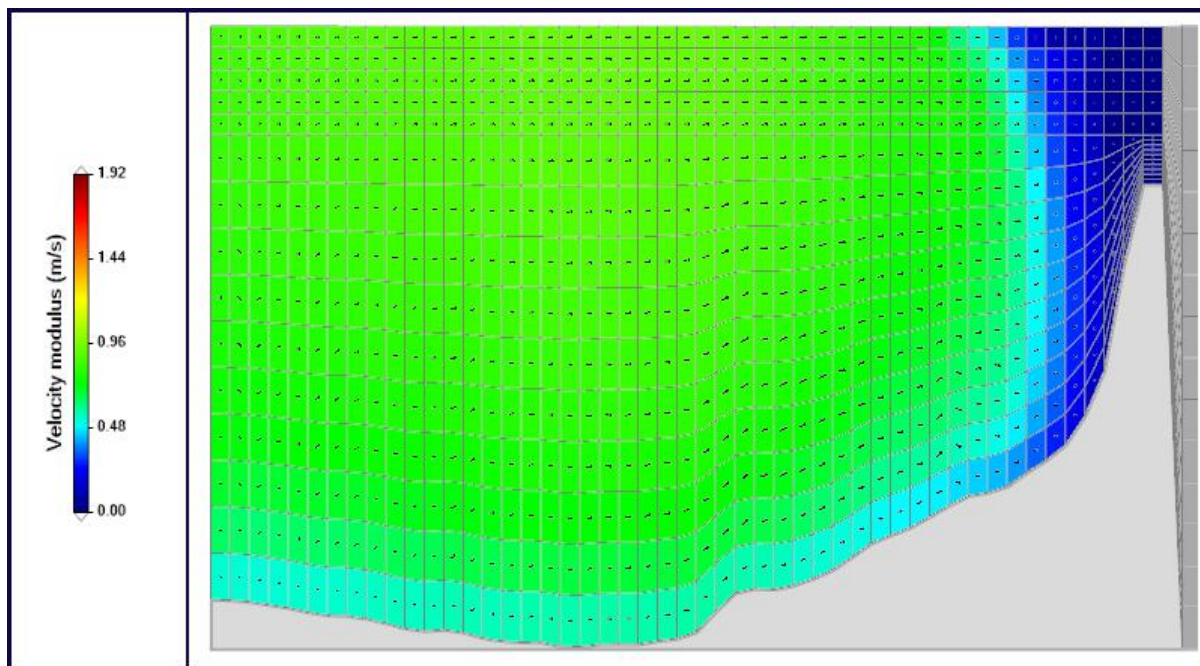


Figure 27 - Velocity modulus (m/s) and field at 12:00:00, "main" model, vertical cut image.

The time series results reveal a noticeable pattern in terms of their spatial distribution and, as such, they were grouped in two sets: results for points at the borders (Figure 28), and results for points at the centre of the domain and points near the discharge (Figure 29).

For the first set (Figure 28), there is a delayed but direct relation to tide height: slightly after the tide reaches maximum or minimum level, the velocity modulus in these locations reaches or approaches zero. The velocity modulus at these points is at its maximum slightly after the midway point between high tide and low tide. This relation shows that points at the borders of the domain are not significantly affected by the tunnel's discharge, as they react only to tide. Immediately after low or high tide, when there is no velocity as a result of tidal effects, so too does velocity approach or reach zero in the borders; when the ebb or flood tide is in its maximum velocity, so is the velocity in the borders.

For the other set (Figure 29), the effect of the discharge is observable. For the point directly in front of the tunnel's discharge point, at the instant when the discharge begins, the velocity modulus also begins to increase, remaining relatively high until the instant when the discharge ends. The velocities in the middle of the domain, however, exhibit behaviour affected both by the discharge and the tide: after a small delay after the beginning of the discharge, the velocity modulus increases until it reaches the absolute maximum, coinciding (albeit, again, with a small delay) with peak ebb tide velocity (the point between high tide and low tide). Afterwards, it decreases to a minimum slightly after low tide, then erratically increases until the discharge stops.

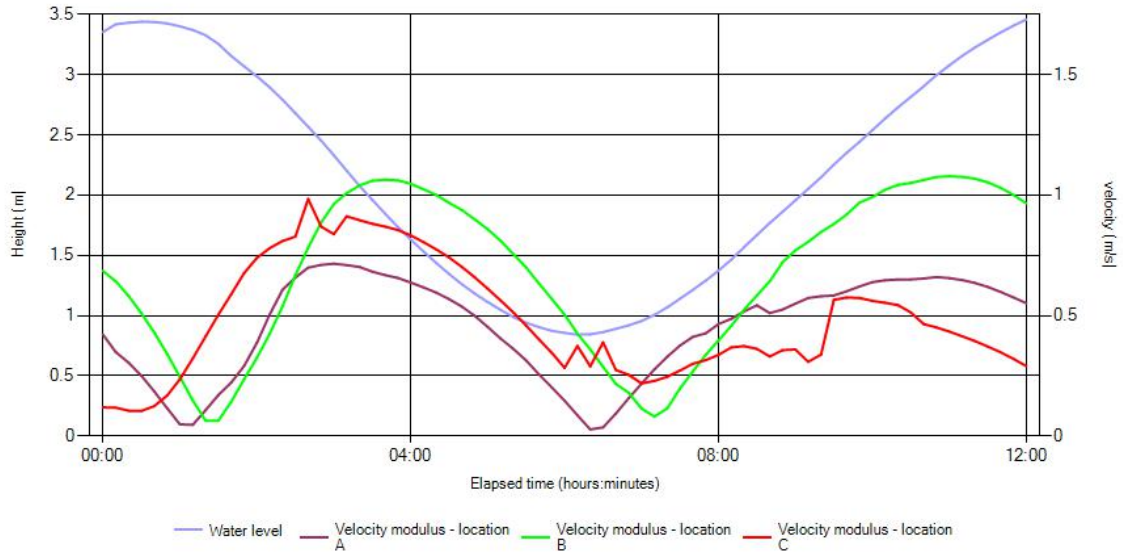


Figure 28 - Velocity modulus (m/s) and water level over time, "main" model, south-west domain border locations.

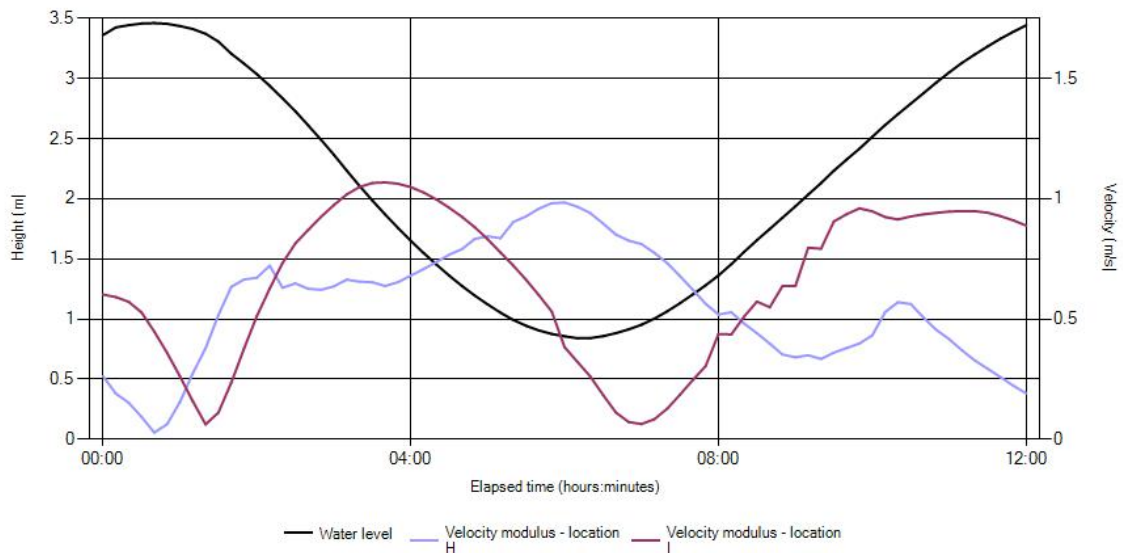


Figure 29 - Velocity modulus (m/s) and water level over time, "main" model, centre of the domain and tunnel mouth locations.

As for the “nested” model, these results can be seen in greater detail. The nature of the results, however, is in great part the same as the "main" model. However, there is one noticeable difference: there seems to be some mathematical inconsistency with the "nested" model's border, which can be seen in the three images presented (Figures 30, 31 and 32): at the non-land borders, cells next to one another show very different velocities in an alternating pattern, which is not an expected result.

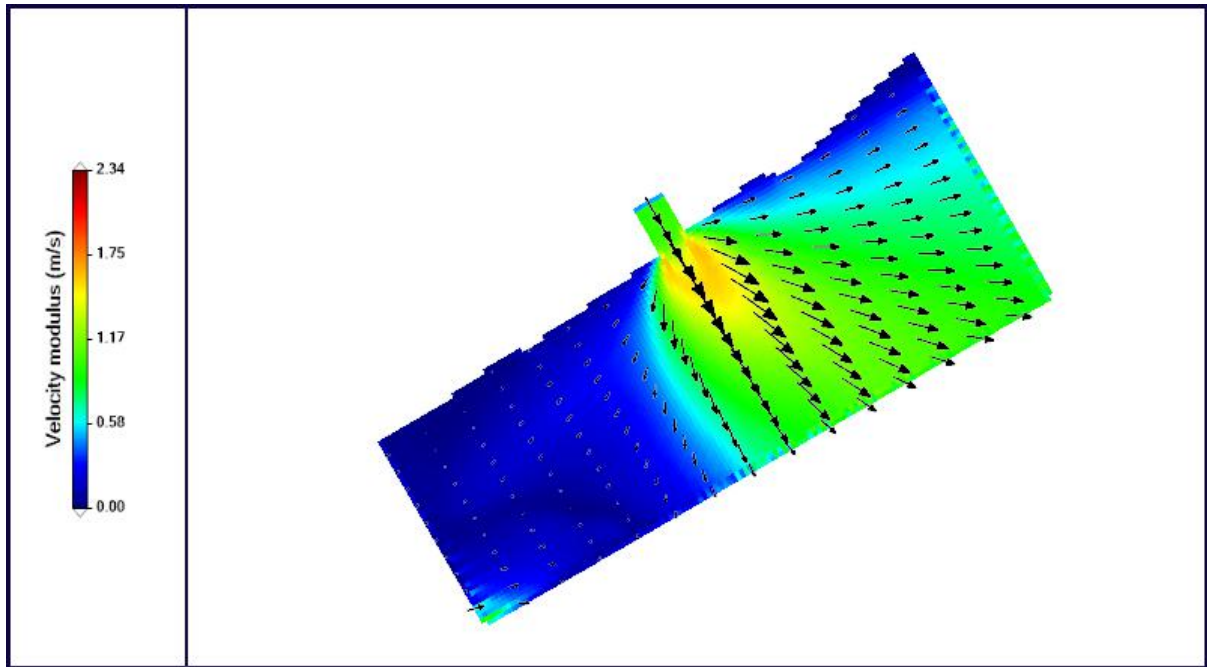


Figure 30 - Velocity modulus (m/s) and field at 10:10:00, "nested" model, horizontal map image.

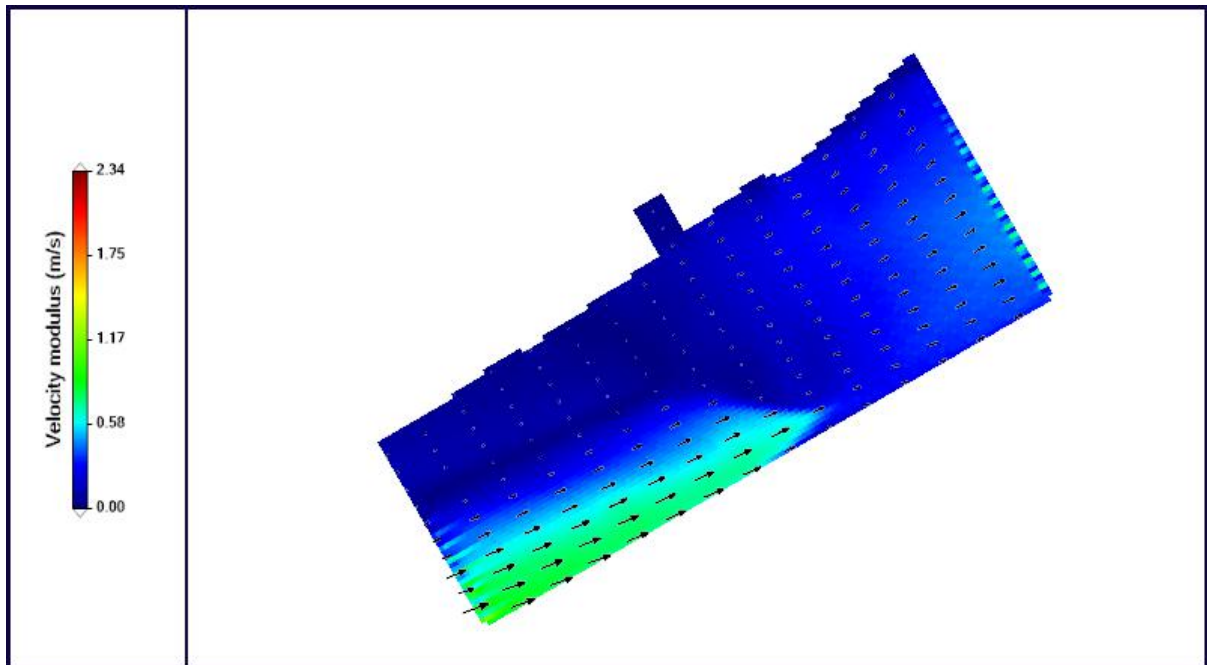


Figure 31 - Velocity modulus (m/s) and field at 11:10:00, "nested" model, horizontal map image.

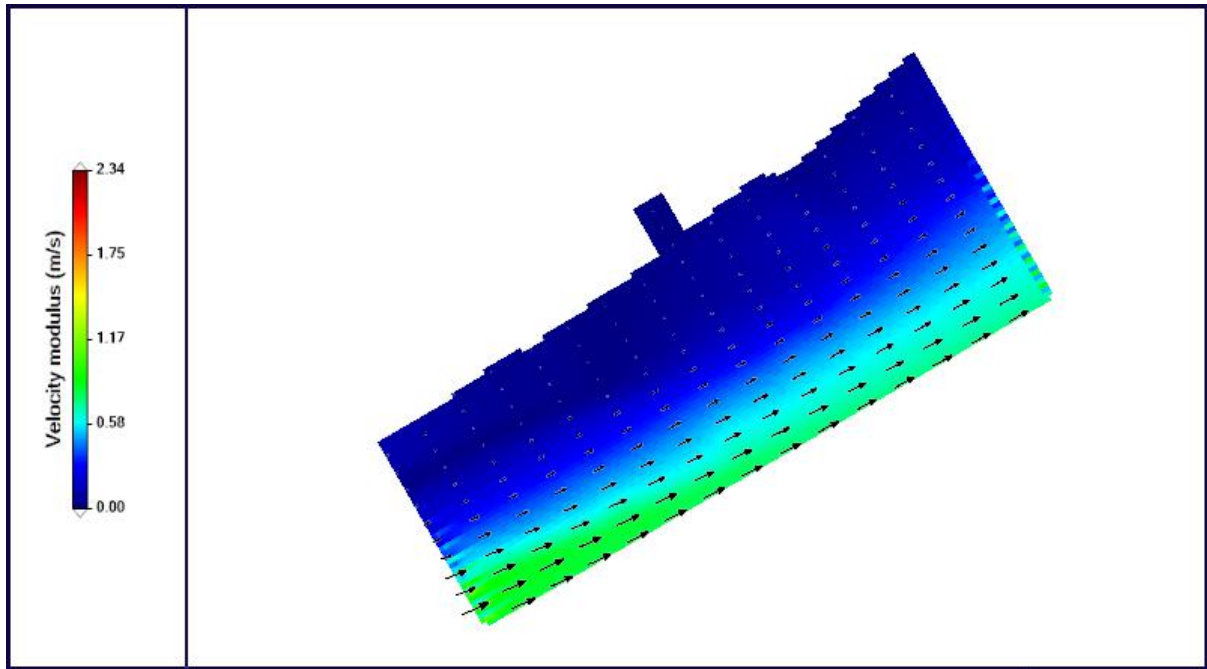


Figure 32 - Velocity modulus (m/s) and field at 12:00:00, "nested" model, horizontal map image.

While similar in behaviour to those of the "main" model, the time series results for the "nested" model display some differences in the values of the velocity modulus. Because the locations in this domain are closer to the tunnel's mouth, the values of the velocity moduli for the border locations (Figure 33) are, in general, higher and show more variance between them, compared to the "main" model. They are also less "smooth", showing once again mathematical inconsistency.

As for the remaining time series results (Figure 34), the location directly in front of the discharge tunnel's mouth seems to be almost exclusively affected by the discharge. At the beginning of the discharge, there is a rapid increase in velocity, followed by a linear but slower increase, until the absolute maximum is reached, which coincides with the half-way instant between the beginning and end of the discharge. What follows is a mirrored behaviour - meaning, there is a slow decrease in velocity, followed by a sharp drop until the discharge stops. The velocity modulus at the centre of the domain appears to behave similarly to the velocity modulus at the discharge tunnel's mouth in the "main" model, likely due to the fact that both locations are very close to one another (location H: 38.7110 N, 9.1240 W; location R: 38.7105 N, 9.1237 W).

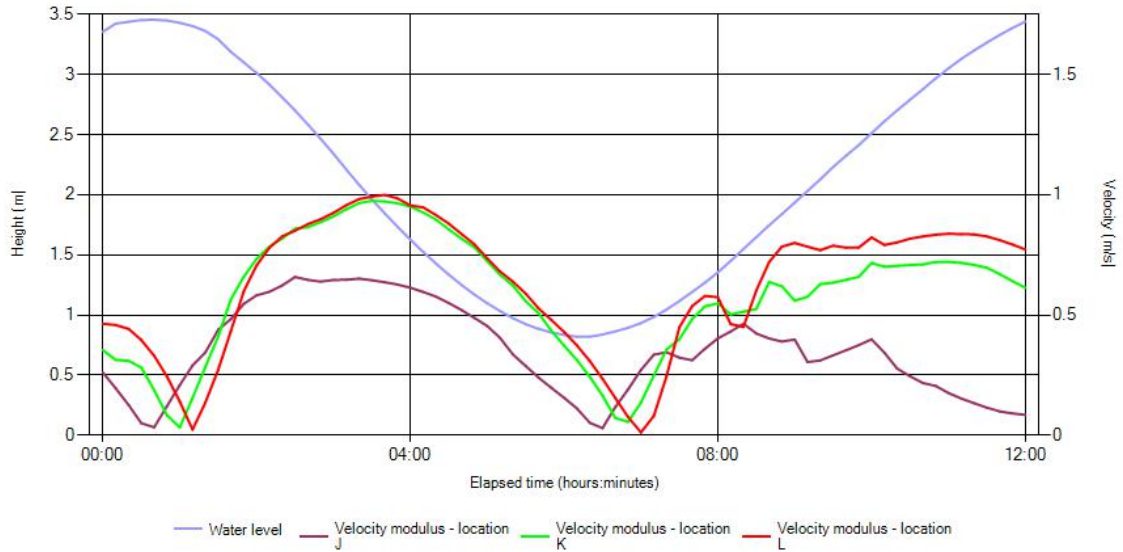


Figure 33 - Velocity modulus (m/s) and water level over time, "nested" model, south-west domain border locations.

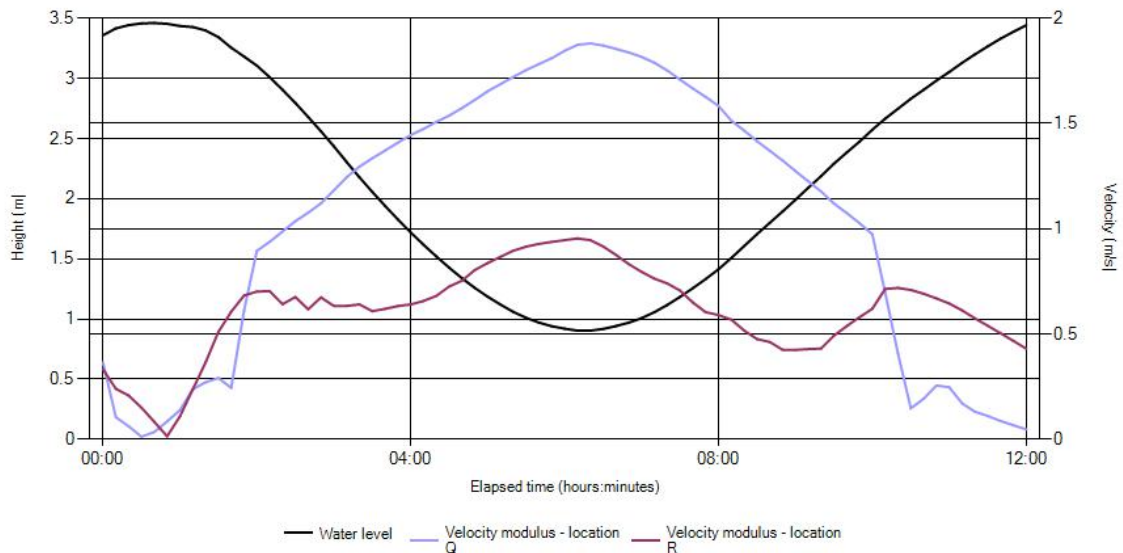


Figure 34 - Velocity modulus (m/s) and water level over time, "nested" model, centre of the domain and tunnel mouth locations.

4.1.2 Water properties

Here, the simulated results for the water properties, namely the concentration of a generic conservative property, are displayed.

As previously described, the model was set so that the water discharge has a generic property dissolved in it, of which the estuary is considered to have an initial concentration of zero.

At 03:30:00, approximately during peak velocity in ebb tide, the concentration plume is clearly defined. In the vertical cut image (Figure 36), the property is seen to be present from surface to bottom. In the horizontal map image (Figure 35), the maximum distance at which the concentration is 50% of the discharge's concentration is 410m, and the maximum distance at which the concentration is 25% of the discharge's concentration is approximately 2225m.

At 07:30:00 (Figure 37), slightly after low tide, the maximum distance at which the concentration is 50% of the discharge's concentration is approximately 347m, and for 25% that distance is approximately 2407m. In the vertical cut image (Figure 38), it is now clear that most of the dispersion of this property occurs at the surface level, as that which was observed at 03:30:00 (the dispersion occurring vertically, from surface to bottom) only happens near the discharge site.

At 09:30:00 (Figure 39), during peak flood tide, the maximum distance at which the concentration is 50% of the discharge's concentration is approximately 410m, and for 25%, that distance exceeds the borders of the domain. An interesting phenomenon is taking place: whereas previously, the tide was sufficient in "removing" this property from a cell and transporting it to an adjacent cell in the direction of the tide, here one can observe that near the coastline there is an area in which a number of cells remain with a relatively high concentration of the generic conservative property.

Finally, at 12:00:00, in both the horizontal map image (Figure 40) and the vertical cut image (Figure 41), there is a noticeable concentration of this property, even if only below 23% or less of the discharge's concentration. This means that a 2 hour period after the end of the discharge is not enough to completely clear out a generic property from the domain, even though at this point, the remaining concentration is very small.

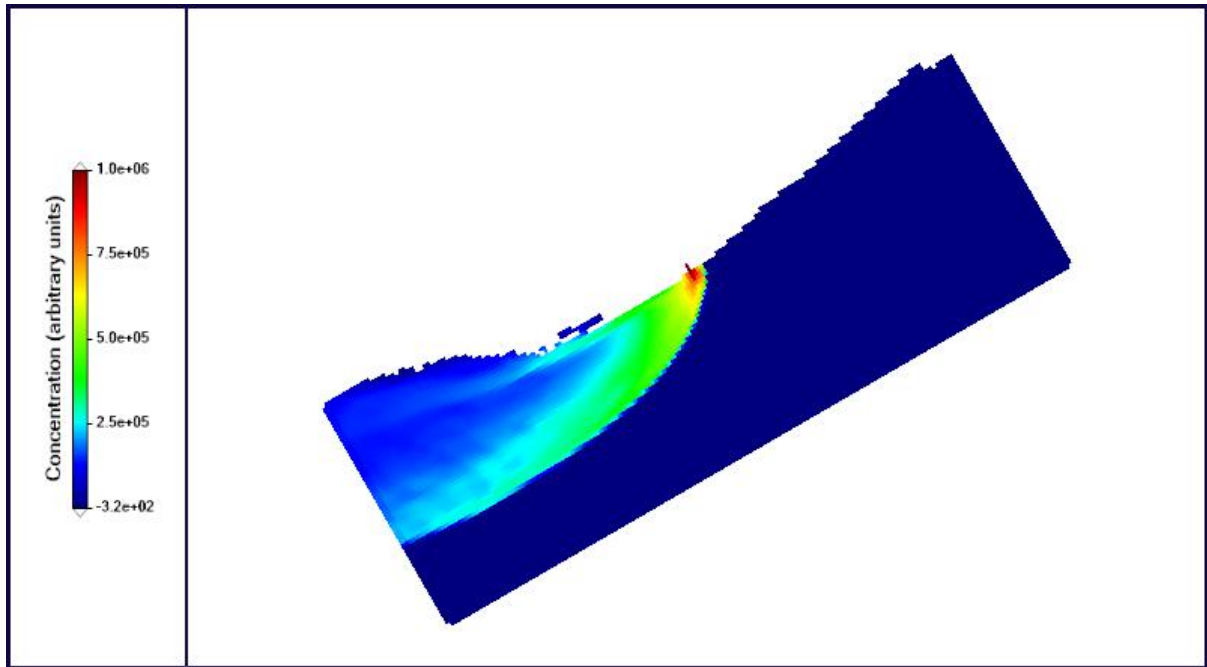


Figure 35 - Generic conservative property concentration at 03:30:00, "main" model, horizontal map image.

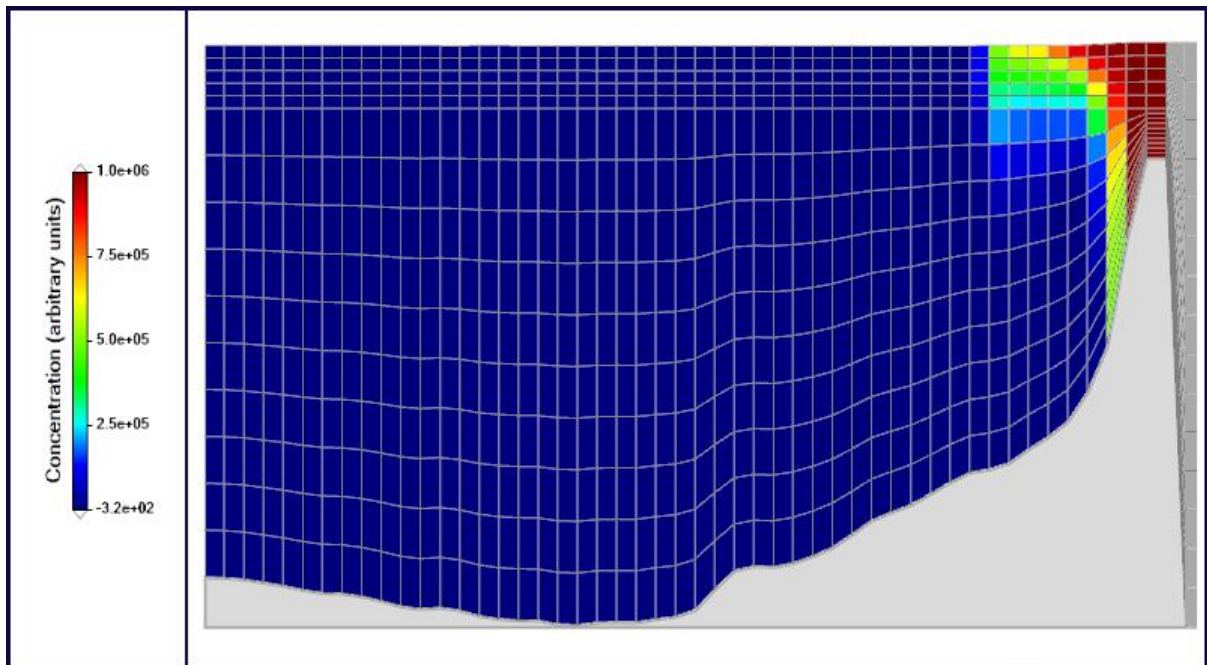


Figure 36 - Generic conservative property concentration at 03:30:00, "main" model, vertical cut image.

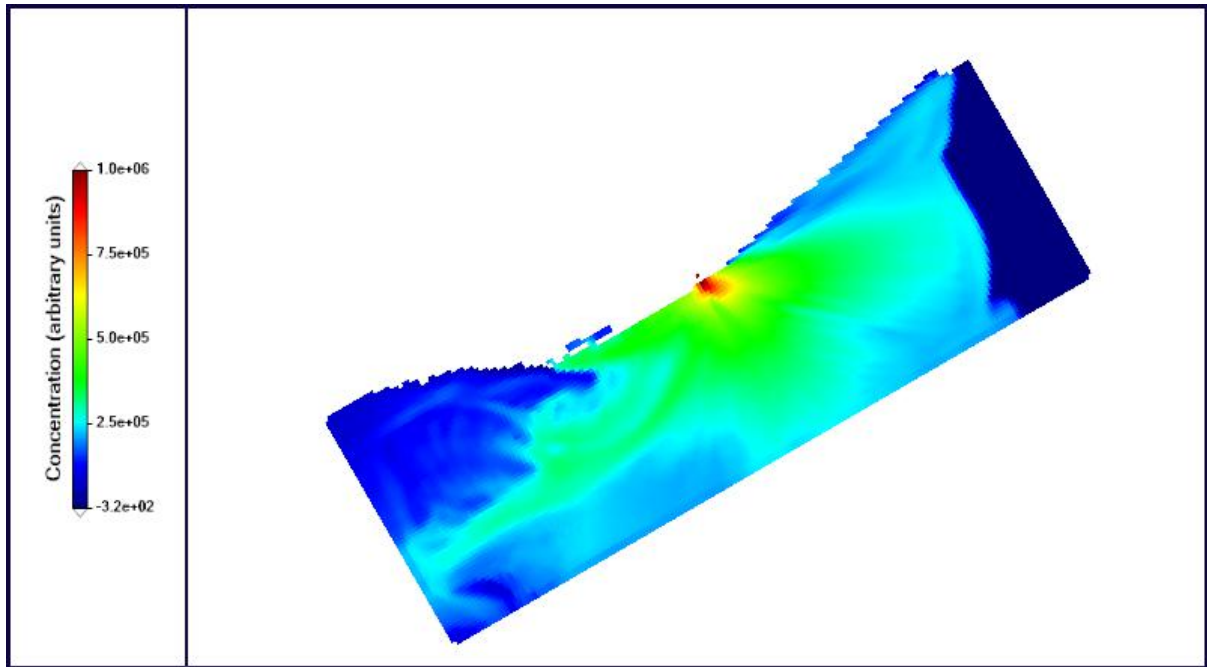


Figure 37 - Generic conservative property concentration at 07:30:00, "main" model, horizontal map image.

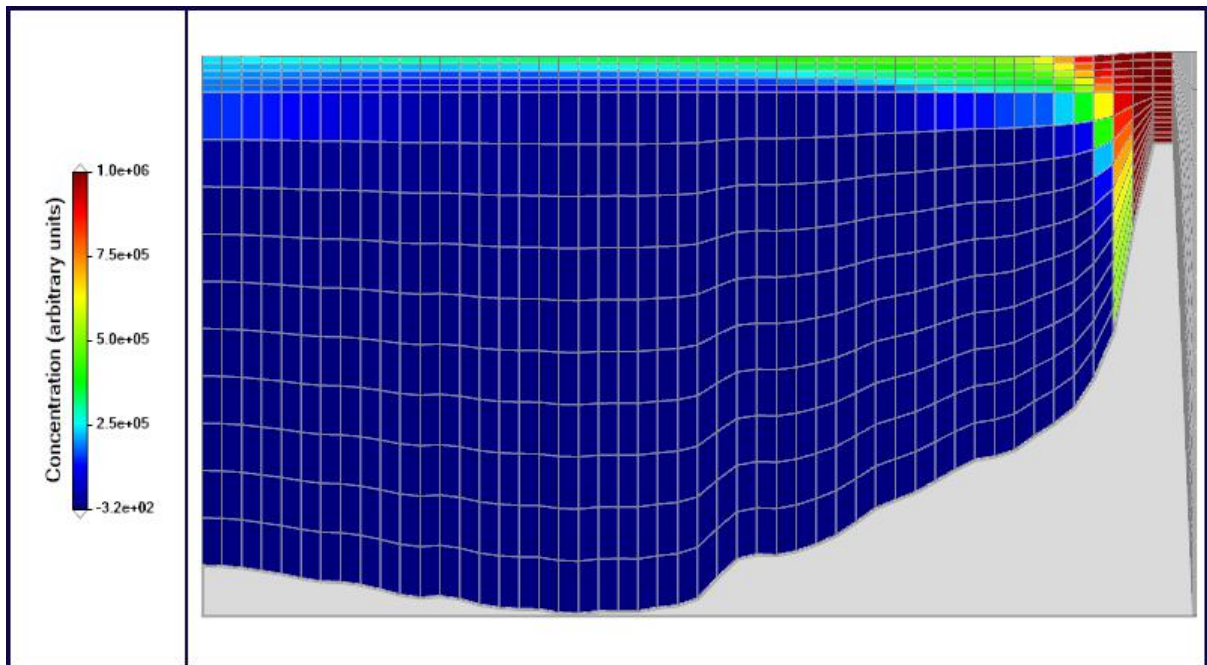


Figure 38 - Generic conservative property concentration at 07:30:00, "main" model, vertical cut image.

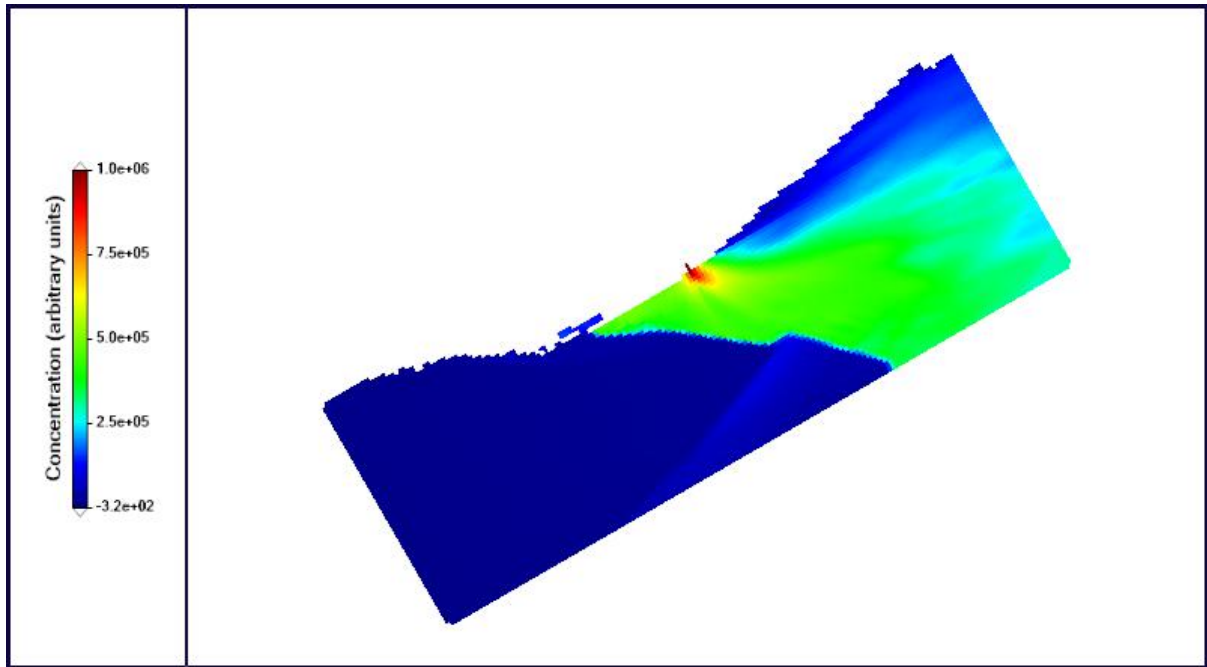


Figure 39 - Generic conservative property concentration at 09:30:00, "main" model, horizontal map image.

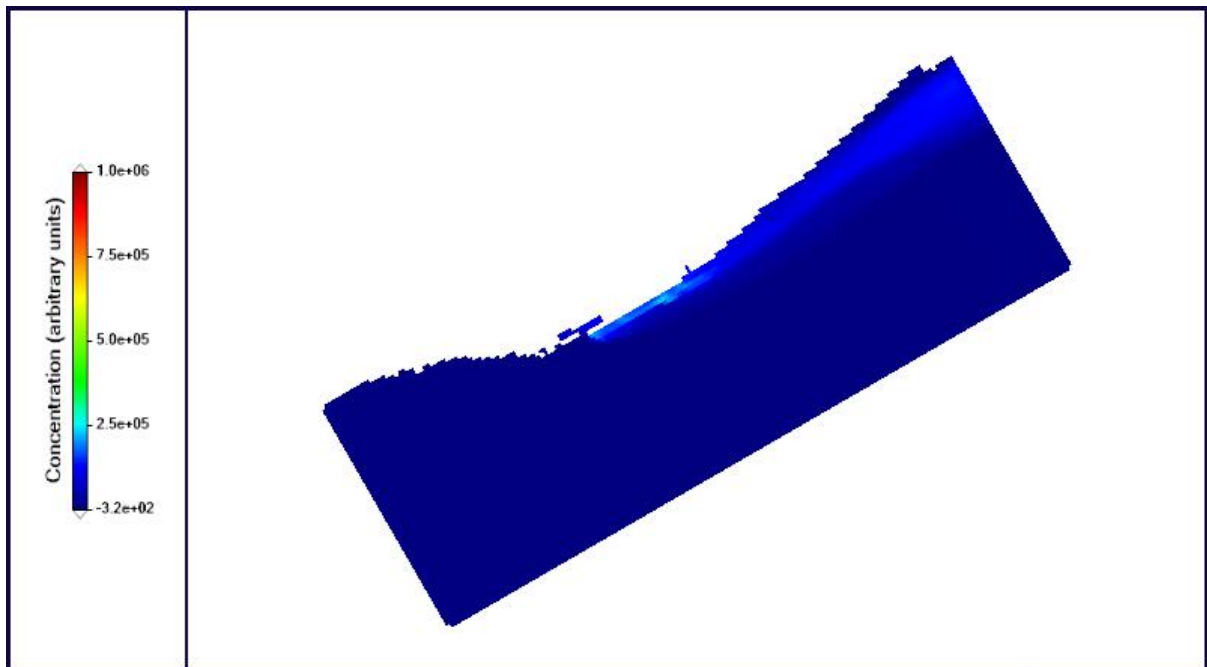


Figure 40 - Generic conservative property concentration at 12:00:00, "main" model, horizontal map image.

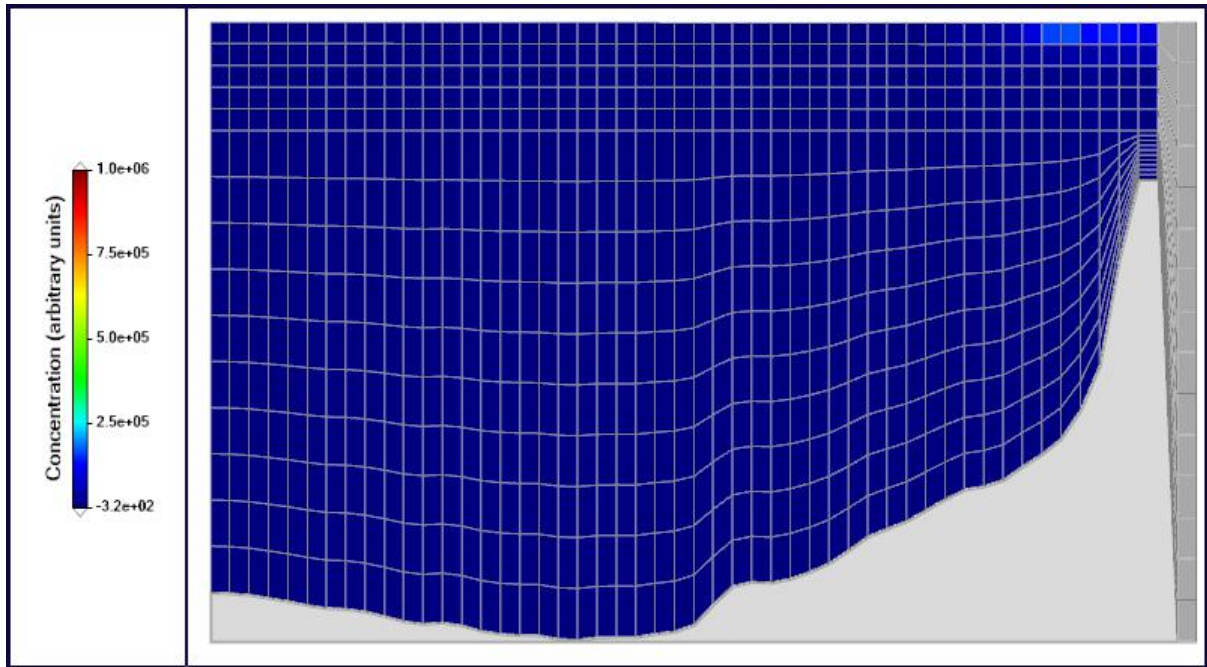


Figure 41 - Generic conservative property concentration at 12:00:00, "main" model, vertical cut image.

As for the time series results, the first ones presented show data regarding the "right" side (north-east) border of the domain (Figure 42). Unlike all other time series locations (Figure 43), with the exception of the one directly in front of the discharge site, the border at the "right" side ends the simulation with concentrations different from zero.

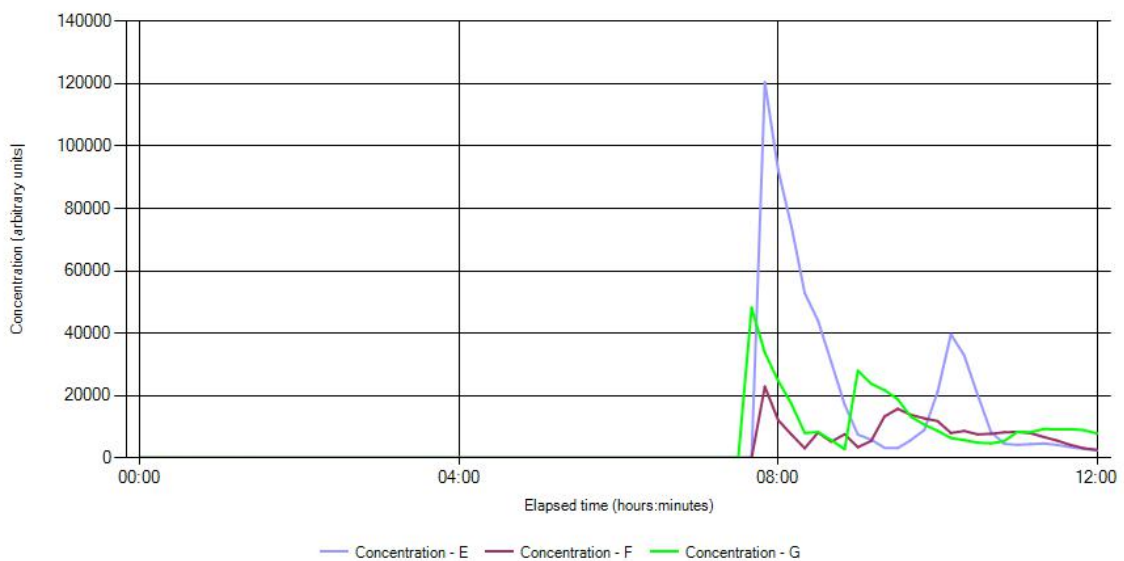


Figure 42 - Generic conservative property concentration over time, "main" model, north-east domain border locations.

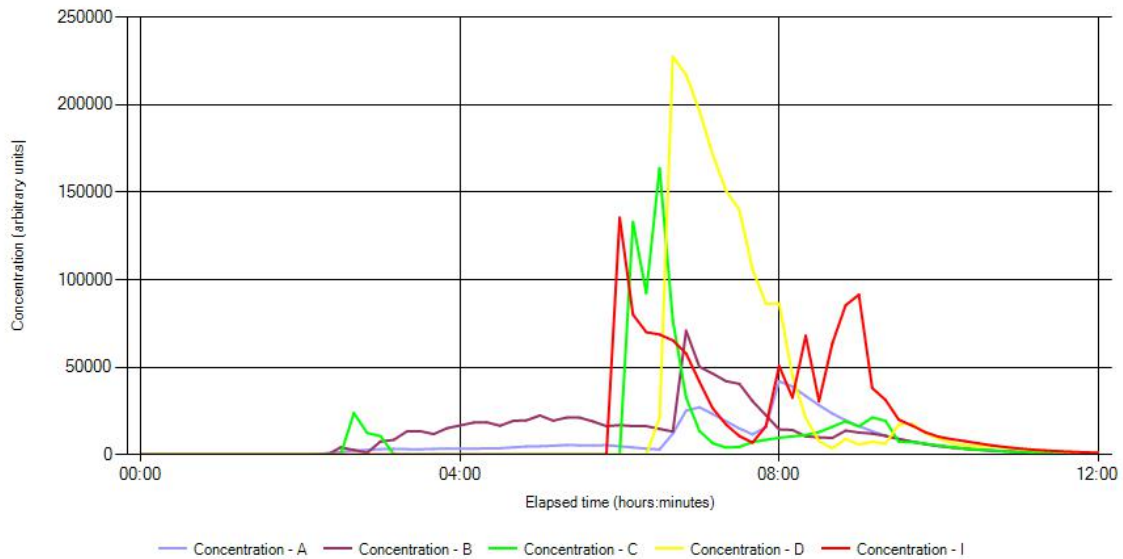


Figure 43 - Generic conservative property concentration over time, "main" model, all locations except north-east border locations and tunnel mouth.

As for the "nested" model, the results are very similar. In this smaller domain, after the 12 hour period (two hours after the end of the discharge), the maximum concentration is below 17.2% of the discharge concentration (Figure 44). In the vertical cut images presented (Figures 45 and 46), once again it becomes clear that the vertical spread of the generic property occurs only near the tunnel mouth, as anywhere further from the coast, it exists only near the surface.

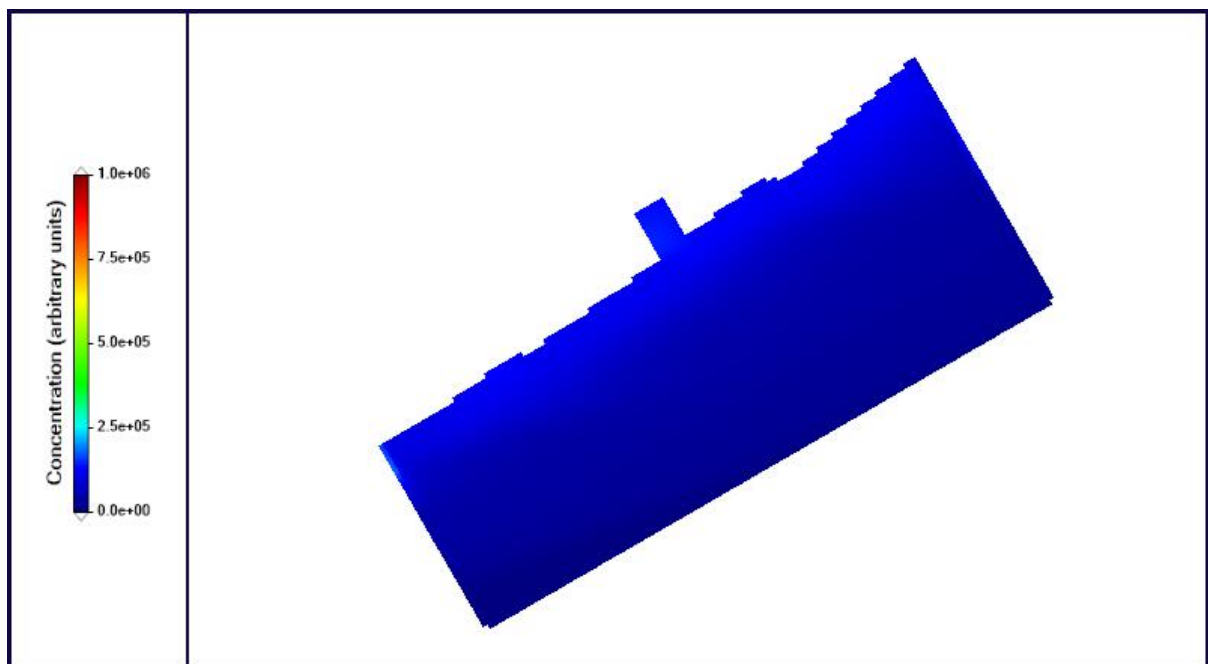


Figure 44 - Generic conservative property concentration at 12:00:00, "nested" model, horizontal map image.

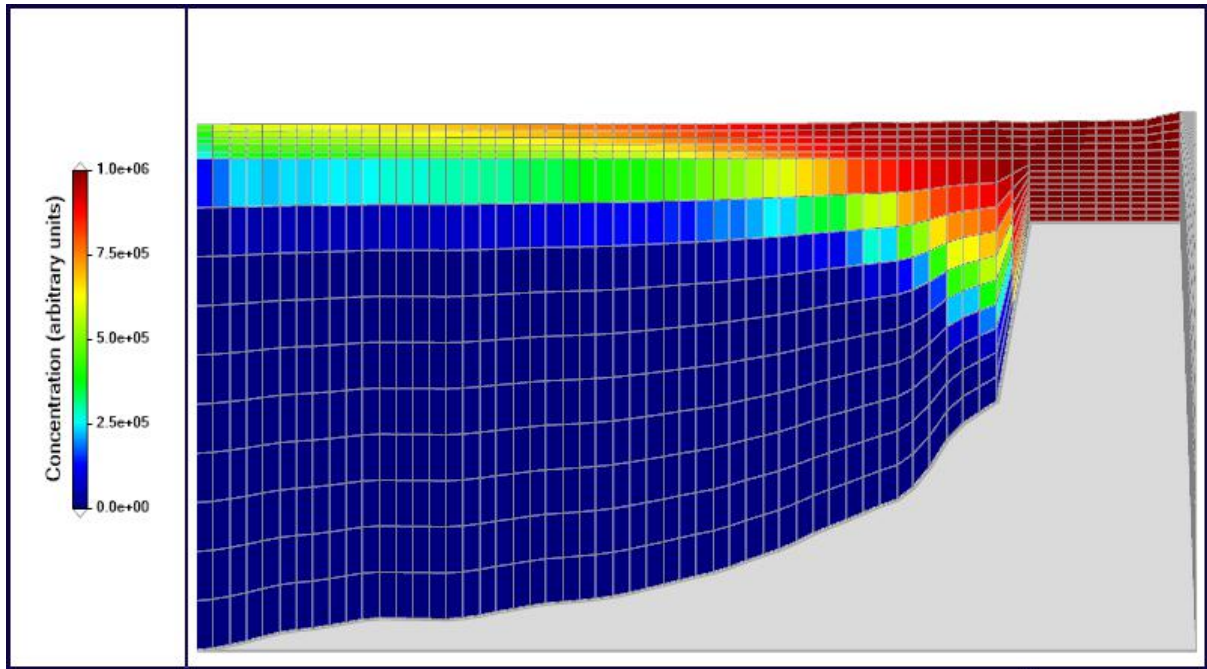


Figure 45 - Generic conservative property concentration at 06:30:00, "nested" model, vertical cut image.

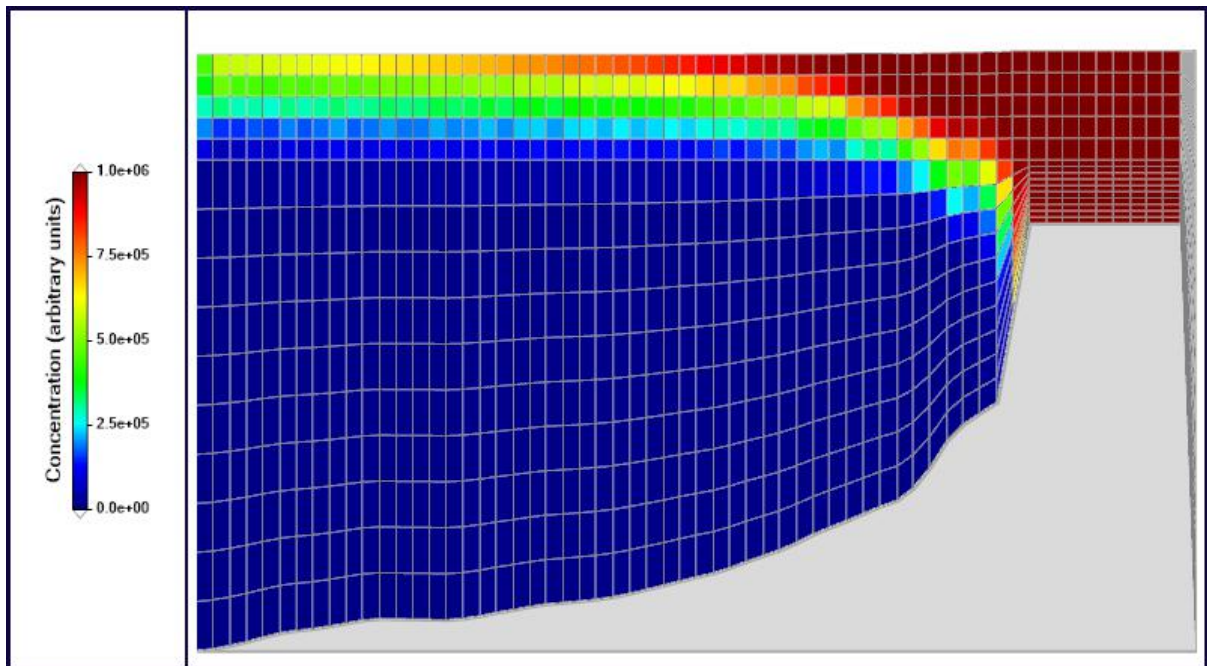


Figure 46 - Generic conservative property concentration at 10:10:00, "nested" model, vertical cut image.

4.2 Morphodynamics

In this section, the results for the sediments (both cohesive sediments and sand classes) as well as for the bottom shear stress are presented. The bathymetry evolution results are not present because the

bathymetry remained unchanged throughout the simulation. All the results present relate to the "nested" model only, as the sediment model was implemented only for that domain.

4.2.1 Shear stress

The results for the bottom shear stress are displayed in this sub-section. The reason that these results are presented here is as a possible explanation as to why there was no bathymetry evolution.

The highest amounts of shear stress are achieved at 03:40:00 (Figure 47), at the point of highest velocity of the ebb tide. As such, as the water level is becoming lower and the velocity modulus is becoming higher, the effects of both the discharge and the tide are affecting the bottom the most than any other time during the simulation. There is also a correlation between shear stress and the amount of sand at the surface, that can be seen when comparing figures 47 and 55.

Afterwards, the shear stress abates (Figure 48), and then becomes relatively uniform throughout the domain until the end of the simulation (Figure 49), at very trace values.

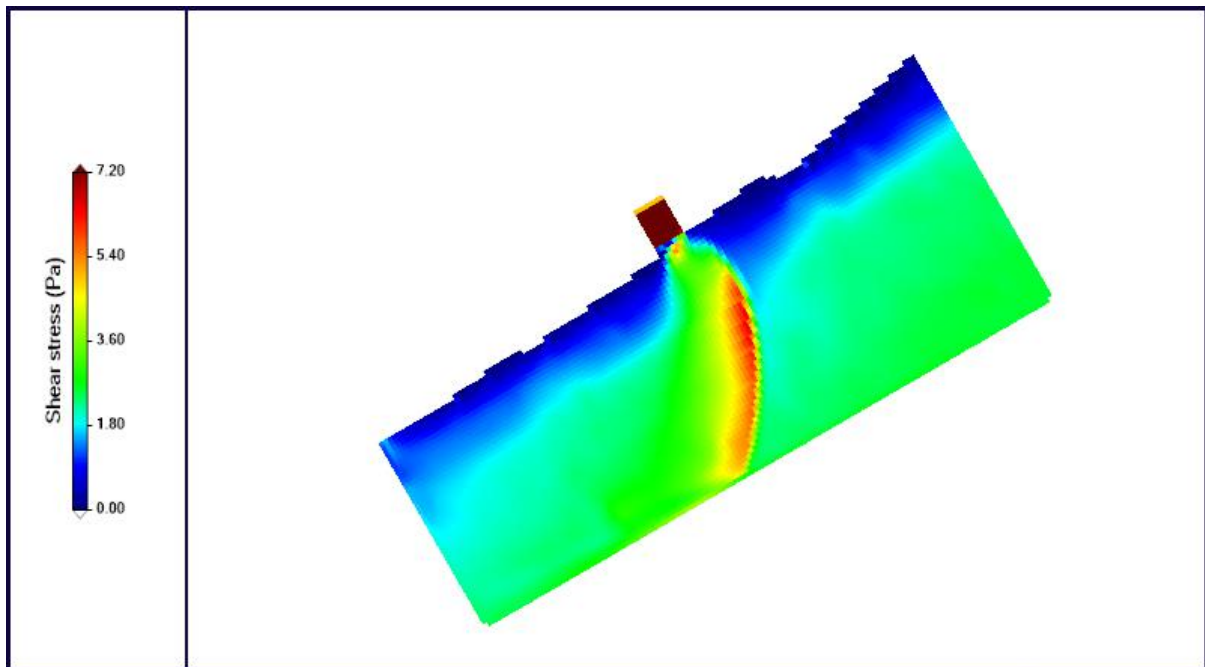


Figure 47 - Bottom shear stress at 03:40:00, horizontal map image.

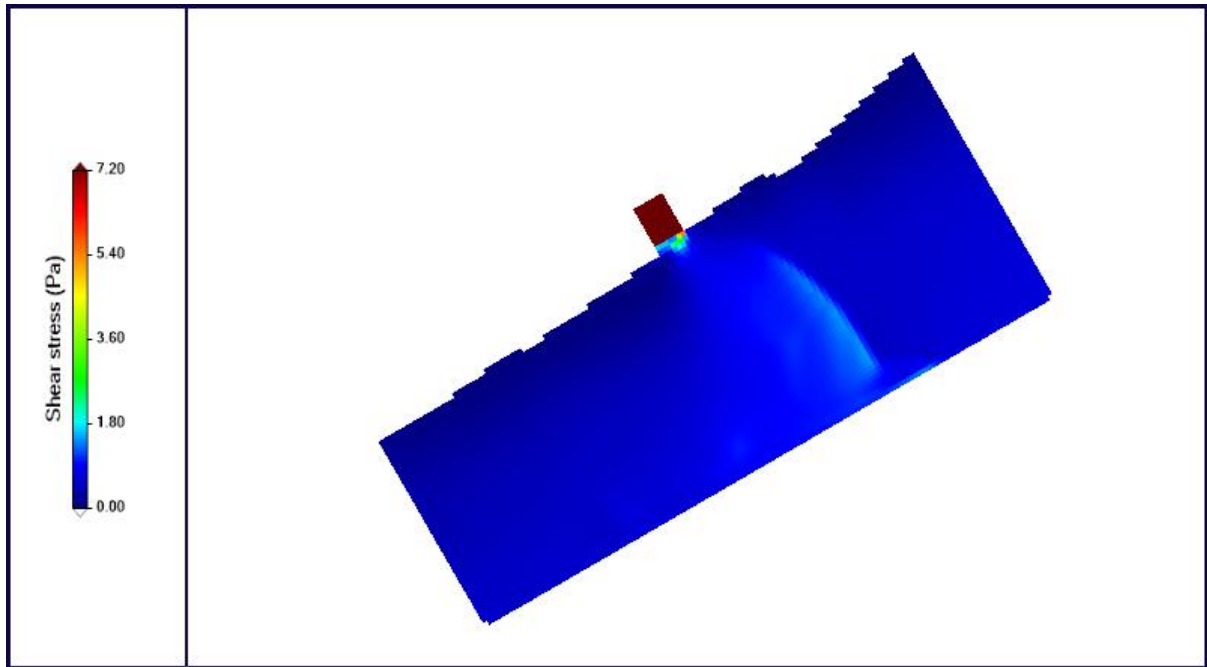


Figure 48 - Bottom shear stress at 05:50:00, horizontal map image.

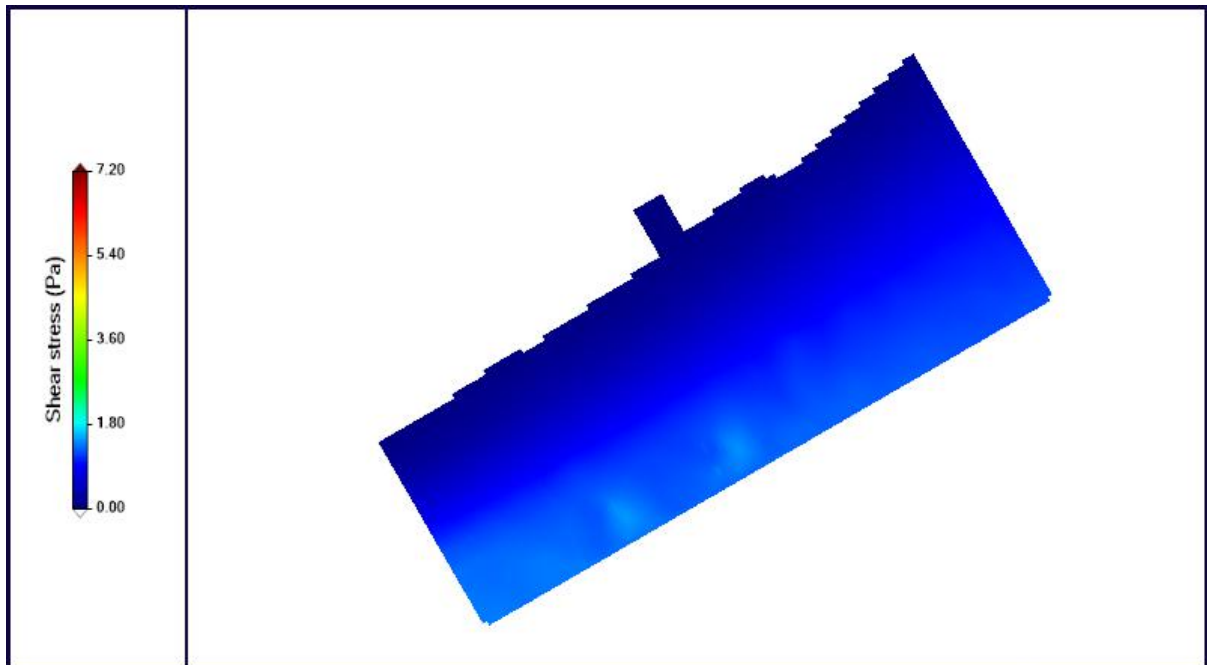


Figure 49 - Bottom shear stress at 12:00:00, horizontal map image.

4.2.2 Cohesive sediments

In this sub-section, the results for the concentration of cohesive sediments in the fluid mud layer (FML) are displayed.

Initially (Figure 50), during high tide, the FML forms over most of the domain, mostly near the shoreline. This was to be expected, as the FML can only be formed when sufficiently low velocities near the bottom exist. During high (in this case) or low tide, the velocity module is very low (approaching zero) and the discharge hasn't yet started, so the FML can form.

Afterwards, up until 06:00:00 (Figure 51), the FML only forms near the shoreline. This would be expected, as anywhere else in the domain (away from the coast) the velocity is increasingly high, therefore not allowing the FML to appear.

Between 06:00:00 and 06:40:00 (Figure 52), the FML starts forming over the whole domain due to the low tide, which means that the velocity modulus is very low. There is a noticeable area, near the discharge site, where the FML cannot form due to the discharge's velocity still affecting the bottom, albeit very slightly.

In the one hour interval between 06:40:00 and 07:40:00 (Figure 53), the observed results are similar to those of the period from the initial moment to 06:00:00. Due to flood tide, the velocity modulus is increasing, and therefore the FML cannot form anywhere, except very near the shore. Comparing those two results shows that the direction of the tide influences on which side of the discharge tunnel the FML form more easily: in case of ebb tide, the FML forms mostly downstream from the discharge site; whereas during flood tide, it exists mostly upstream.

Finally, from that point until the end of the simulation at 12:00:00 (Figure 54), the FML is almost completely cleared from the domain, by being flushed out almost entirely by the water flow. There is a marginal amount near the shoreline.

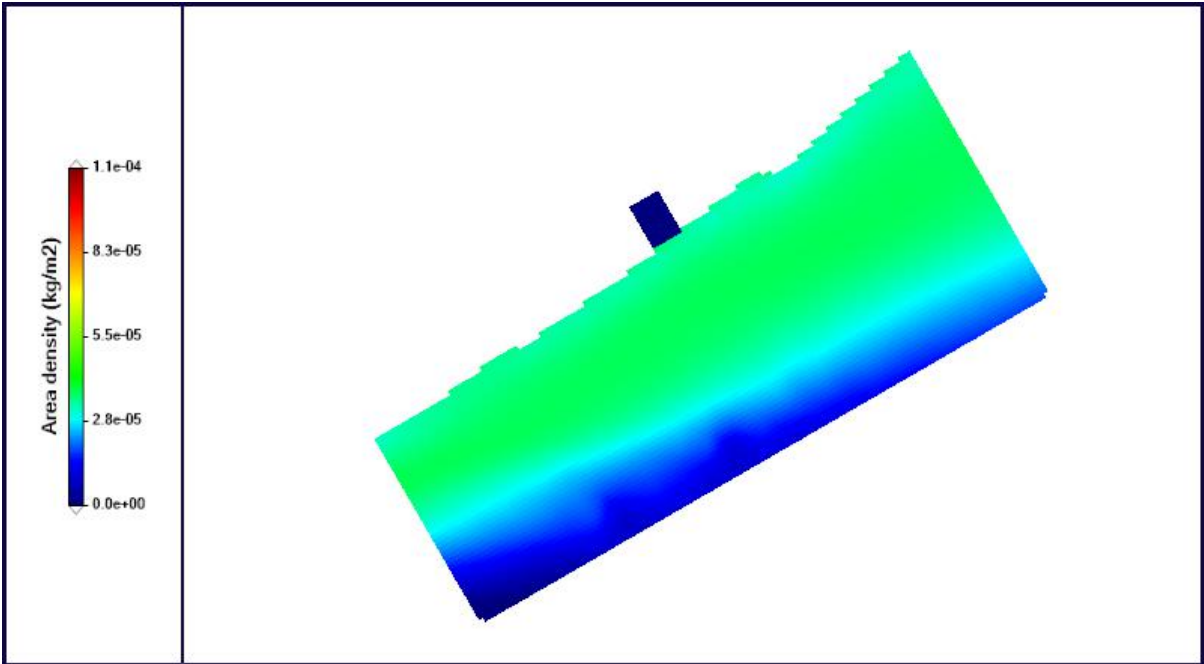


Figure 50 - Fluid mud layer at 00:40:00.

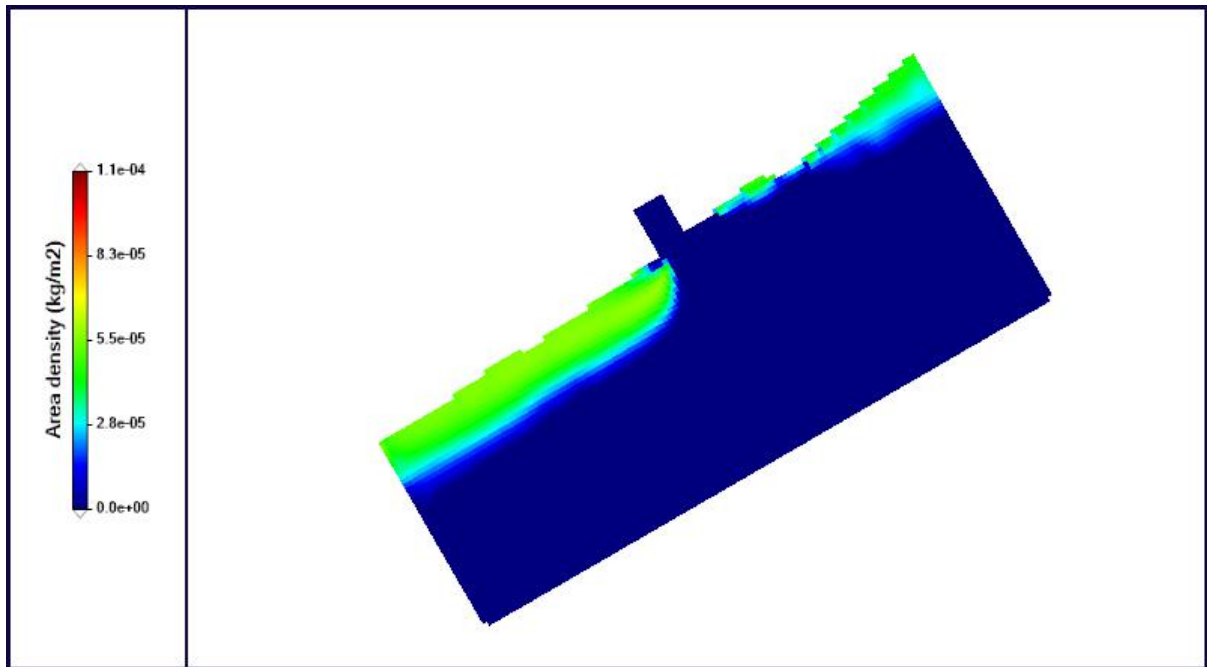


Figure 51 - Fluid mud layer at 06:00:00.

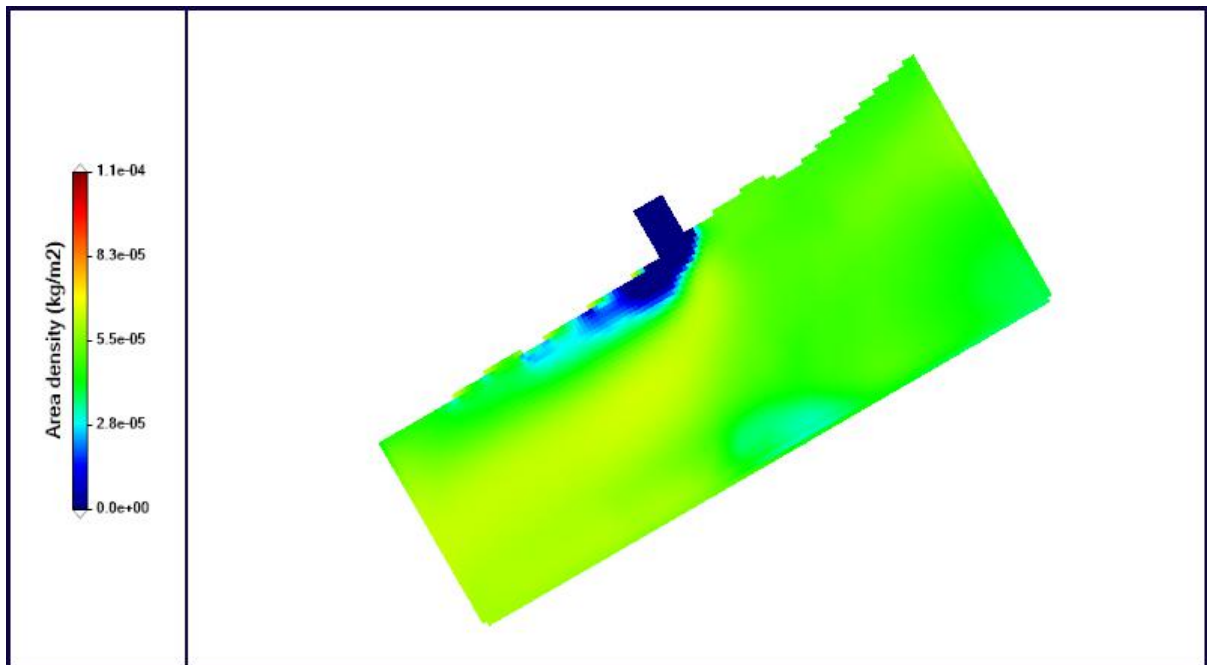


Figure 52 - Fluid mud layer at 06:40:00.

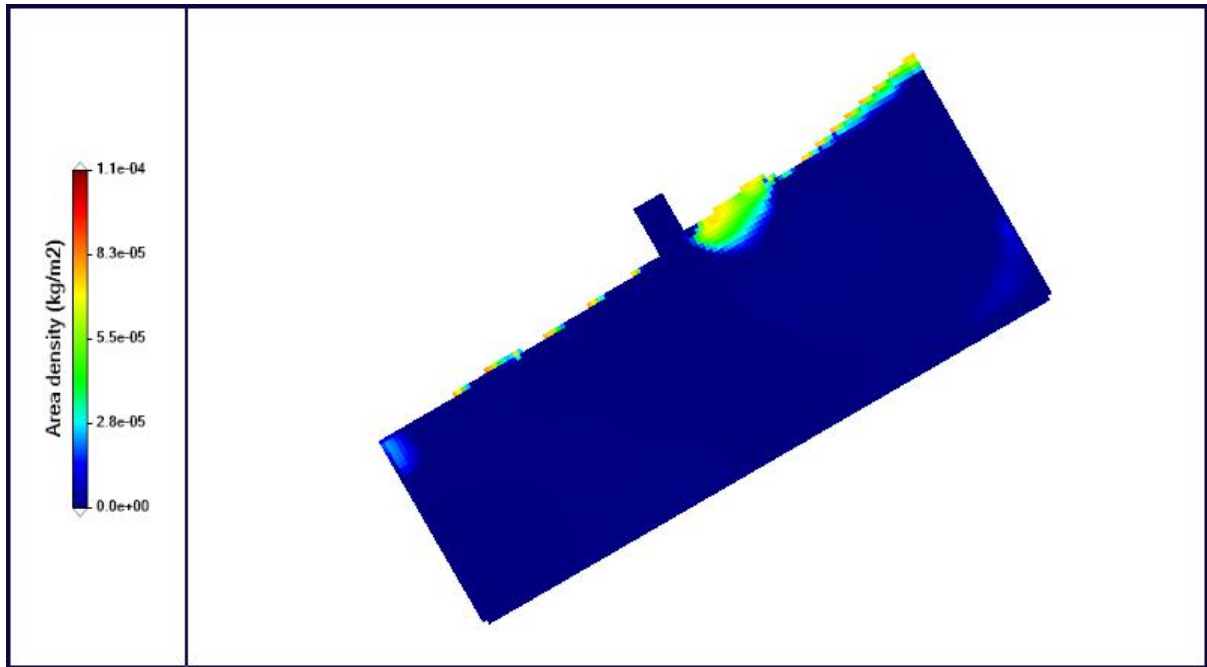


Figure 53 - Fluid mud layer at 07:40:00.

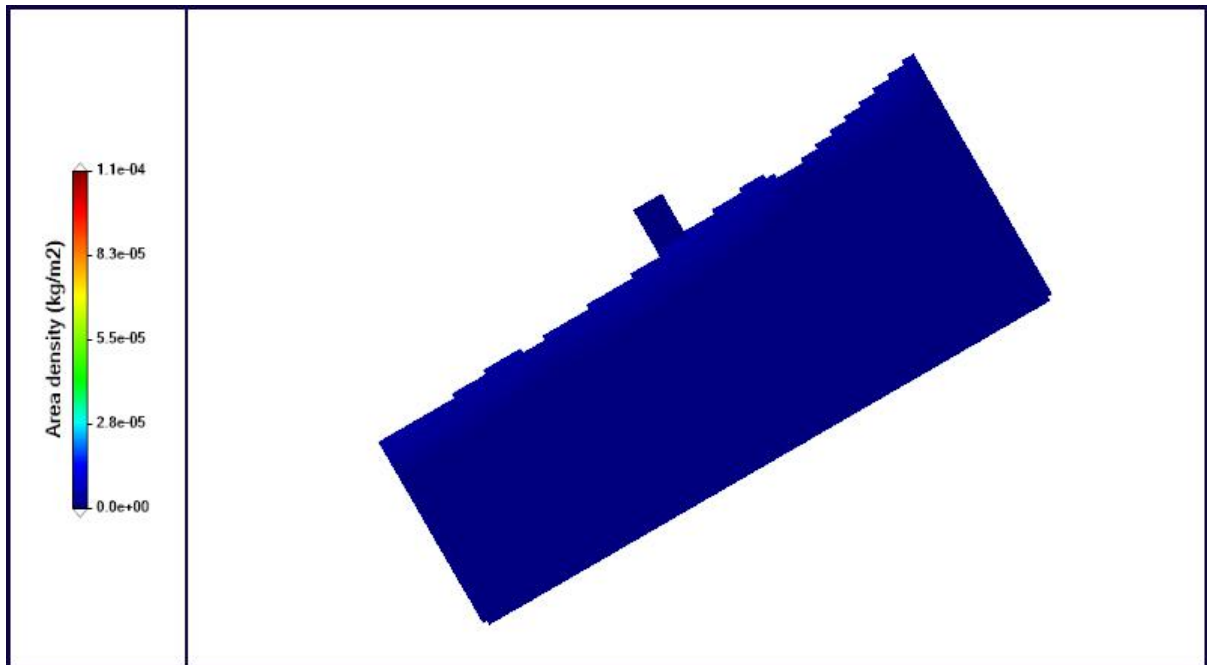


Figure 54 - Fluid mud layer at 12:00:00.

4.2.2 Sand classes

Here, the results regarding the spatial distribution of the concentration of very fine sand (class 1) are presented, as it was the only sand class that was affected throughout the simulation.

Initially, sand is not being eroded from the bottom, and therefore there is no sand in the water column. However, from 02:00:00 until 05:20:00, there is sand in the water column, being eroded by the shear stress of the water flow of the tide (at this point, flood tide) as well as of the water discharge from the tunnel. During this interval, at one point there is even sand at the surface, as seen in Figures 55 and 56.

For 10 minutes, until 05:30:00, there's once again no sand in the water column. However, between 05:40:00 and 05:50:00 (Figure 57), there's another instance of sand being eroded and going to the water column.

From 06:00:00 to 07:50:00, there's again no sand in the water column. From 08:00:00 until the end of the simulation (Figure 58), there is again sand in the water column near the bottom of the domain.

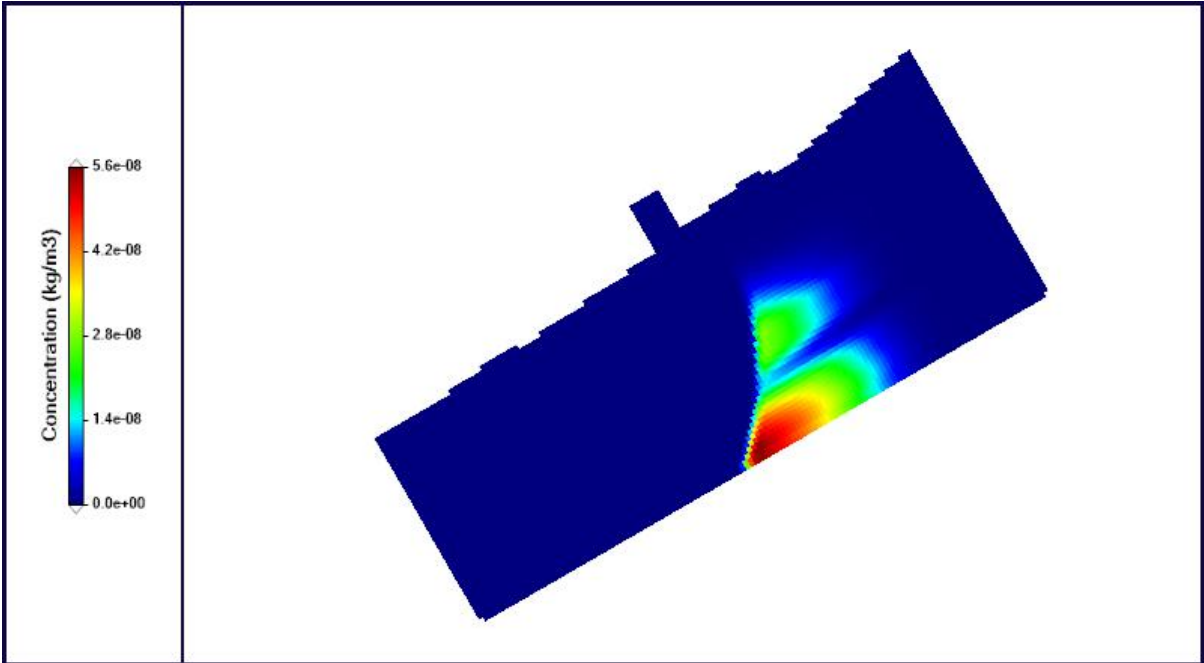


Figure 55 - Concentration of very fine (class 1) sand at 03:40:00, horizontal map image.

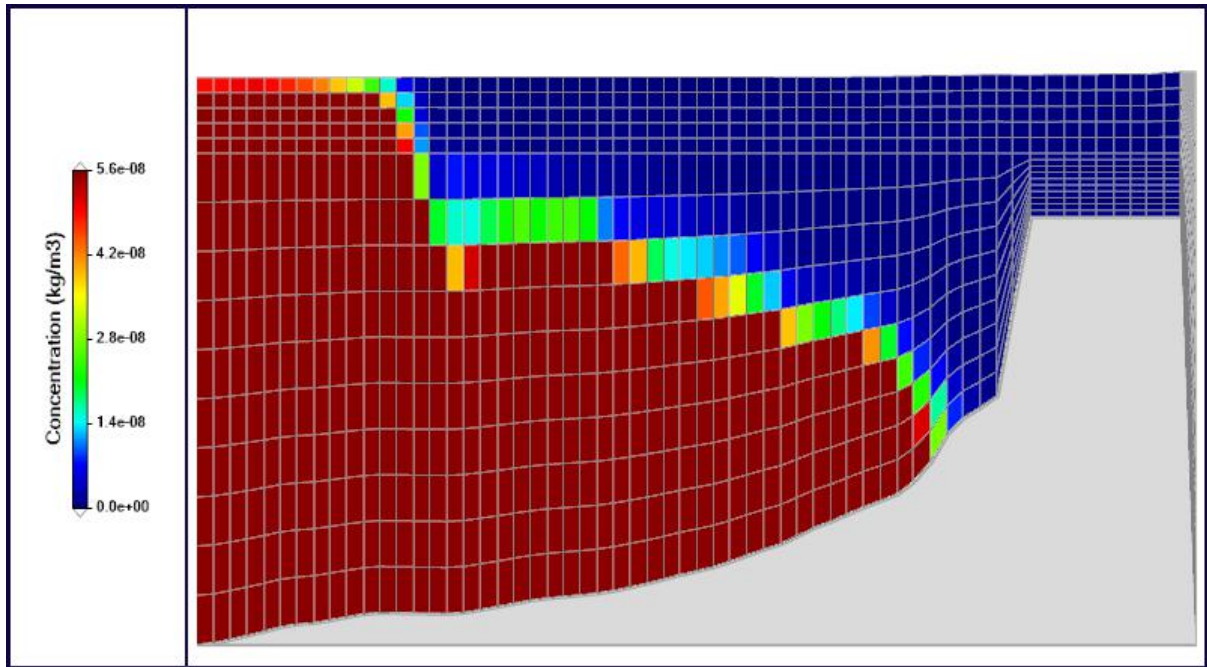


Figure 56 - Concentration of very fine (class 1) sand at 03:40:00, vertical cut image.

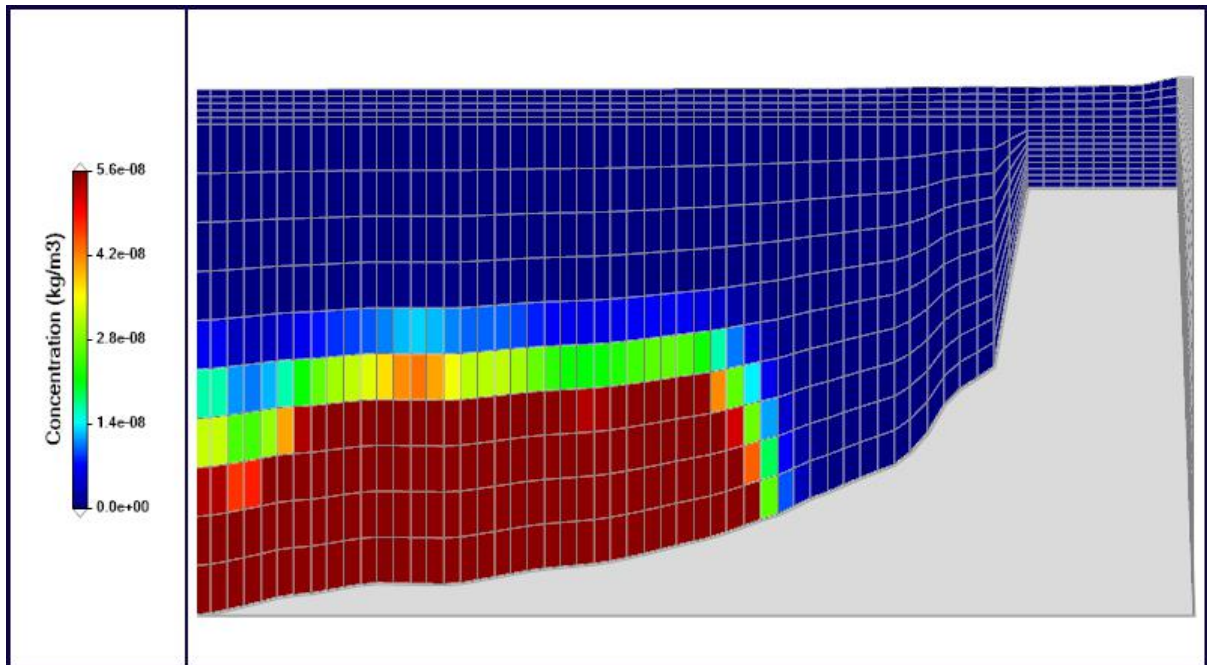


Figure 57 - Concentration of very fine (class 1) sand at 05:50:00, vertical cut image.

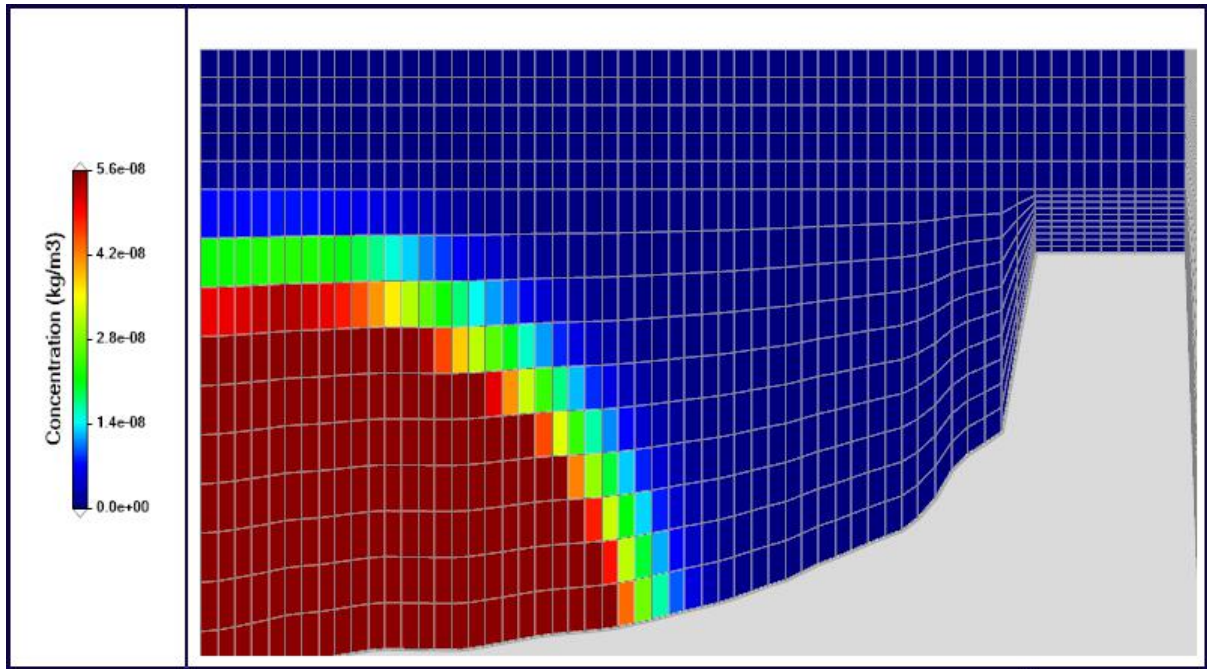


Figure 58 - Concentration of very fine (class 1) sand at 12:00:00, vertical cut image.

5. Conclusions and future work

6.1 Conclusions

A three-dimensional computer model was used to model the discharge of an emergency floodwater load into the Tagus river's estuary. The simulated outputs were the water velocity modulus and field, the water level (as it relates to the tide and the water discharge), a generic conservative property (diluted in the discharge), the cohesive sediments, different sand classes (non-cohesive sediments), and the bottom shear stress.

The hydrodynamics were successfully simulated, whereas the morphodynamics had a lesser degree of success, mostly because the fact that more accurate data was not available and as such a schematic case was set-up.

In the PGDL report, such an analysis is not present, as the only modelling done in that report related to the discharge before being released into the estuary. As such, this work adds to knowledge about the projected tunnel, as it may allow planners to better understand the impacts that may come from this project, should it indeed be built.

The effects of the tunnel's discharge on the velocity modulus were almost exclusively at the surface, with the sole exception of the previously described wedge's vertical effect. In terms of surface extension, the affected area was, at its highest extension, in an approximate radius of 1150m. After the 12 hours of the simulation, however, the tunnel's discharge does not affect the velocity modulus anywhere in either domain.

As for the results regarding the concentration of a generic conservative property, once again, the effect of the discharge is mostly horizontal, with the exception of the area very near (indeed, adjacent to) the discharge site. At the end of the simulation, within the "nested" domain, the highest remaining concentration is 17.2% of the concentration at the discharge, and only very near the coast, as anywhere else in this domain, the concentration is negligible.

In regards to shear stress, at its peak, it reached approximately 7 Pa in the zone directly ahead of the discharge site for approximately 2 hours; for the remaining simulation, it stayed nearly uniform in all of the domain, between 0 to 1.8 Pa.

The fluid mud layer forms, at two different moments, over almost the entire domain; however, throughout most of the simulation (for 9 hours and 30 minutes out of the 12 hour simulation), the fluid mud layer is only present next to the shoreline. At most, this fluid mud layer has an average surface density of approximately 60 mg/m².

As for the results regarding non-cohesive sediment, or sand, only very fine (class 1) sand, with $d_{50}=0.2\text{mm}$, was affected; this means that at most only the top 0.4m of the sediment column was impacted by the combined effect of the discharge and the tide, for the 12 hours duration. This sand actually reached the water surface for approximately 2 hours (during the discharge), whereas throughout the rest of the simulation it continually and cyclically eroded and deposited. All of these effects occurred away from the coast, near the south-eastern border of the domain. The removed sand was not in enough quantity to affect the bathymetry.

These results show that most of the hydrodynamic and morphodynamic impacts that the discharge has on this part of the Tagus river's estuary are either localized, non-existent (or nearly non-existent) at the end of the 12 hour period, or both.

Generally speaking, it was observed that the discharge's impact is mostly felt at the water surface; the only exception seems to occur in the zone directly in front of the discharge, when tidal velocity is at maximum (peak ebb tide or peak flood tide).

6.2 Future work

As information regarding sediment quantity and quality in this particular area of the Tagus river's estuary is not available, the parameters regarding sediments are not accurate, but instead a generic model distribution. Therefore, the results regarding the distribution of the different sand classes, as well as cohesive sediment, should not be taken as a realistic prediction but as a base scenario in which the effects of the tunnel's discharge can be felt. At any rate, because the effect of the discharge on the bathymetry and sediments is so minimal (which is verified by the fact that the simulated bottom shear stress is very small), the effects are negligible either way. In other words, because the effect of the tunnel's discharge on the sediment column is so minimal, it is not highly relevant if the column is realistically modelled. As such, if data on the distribution of sediments in the Tagus estuary becomes more precise and available, a more accurate simulation could be developed and studied.

Another concern relates to the fact that the tunnel in this model is under hydrostatic conditions (free surface) rather than under pressure, which would be the realistic conditions of the flow in the tunnel. This means that the velocity in the tunnel's mouth is not correctly modelled, and there is some error associated with this approximation. In the future, using Bernoulli's equation, estimating the velocity time series for the discharge and using the resulting velocity profile for the simulation rather than assuming hydrostatic conditions for the discharge could yield more realistic and reliable results.

As a final remark, it is important to keep in mind that this study is preliminary and should be interpreted as such. As has been repeated throughout this thesis, it is a general study largely based on what information has been made available by the Lisbon Municipality.

References

Campuzano, F.J., Leitão, P.C., Gonçalves, M.I., Marín, V., Tironi, A. (2008). Hydrodynamical vertical 2D model for the Aysén fjord, Perspectives on integrated coastal zone management in South America, IST Press.

Carta de Vulnerabilidade ao Risco de Inundação, no concelho de Lisboa (2017). Riscos da cidade - Câmara Municipal de Lisboa, http://www.cm-lisboa.pt/fileadmin/VIVER/Seguranca/Protecao_Civil/ficheiros/Carta_de_Vulnerabilidade_ao_Risco_de_Inundacao.pdf

Fernandes, R. (2005). Modelação Operacional no Estuário do Tejo, Dissertação para a obtenção do grau de Mestre em Ecologia, Gestão e Modelação dos Recursos Marinhos, Instituto Superior Técnico, Universidade Técnica de Lisboa.

Fofonoff, N. P., Millard, R. C. (1983). Algorithms for computation of fundamental properties of seawater, Unesco technical papers in marine science.

Franz, G., Leitão, P., Pinto, L., Jauch, E., Fernandes, L., Neves, R. (2017). Development and validation of a morphological model for multiple sediment classes, International Journal of Sediment Research

Guerreiro, A., Monteiro, A., Ferreira, F., Braunschweig, F., Simões, J., Guimarães, J., Matos, J. S., Estudante, M., Pinheiro, M., Ribeiro, P., Oliveira, R. P., Leboeuf, Y., Fernandes, Z. (2015). Plano Geral de Drenagem de Lisboa 2016 - 2030, CML. http://www.cm-lisboa.pt/fileadmin/PARTICIPAR/plano_drenagem/PGDL2_RFinal_V43.pdf

Mateus, M., Oliveira, A. P. (2013). A numerical study of CO₂ dynamics in the Tagus estuary, Ocean modelling for coastal management - Case studies with MOHID, IST Press.

MOHID Modelling System Description.

Pierini, J.O., Marcovecchio, J., Campuzano, F., Perillo, G.M.E (2008). Evolution of salinity and temperature in Bahía Blanca estuary, Argentina, Perspectives on integrated coastal zone management in South America, IST Press.

Pincha, J. P., Monteiro, F., Martins, C. F., Cappelletti, M., Duarte, R. O. (2014). Fotogaleria: Chuva intensa provoca inundações em Lisboa, *Observador*, <http://observador.pt/2014/09/22/chuva-intensa-provoca-inundacoes-em-lisboa/>

Pinto, L., Mateus, M., Ascione, I., Franz, G., Neves, R. (2013). Modelling mussel growth in Tagus estuary: a preliminary approach, Ocean modelling for coastal management - Case studies with MOHID, IST Press.

Rodrigues, J. (2015). The Tagus estuarine plume variability: impact in coastal circulation and hydrography, Dissertação apresentada à Universidade de Aveiro para cumprimento dos requisitos necessários à obtenção do grau de Mestre em Meteorologia e Oceanografia Física.

Urban soil sealing in Europe (2011). European Environment Agency, <https://www.eea.europa.eu/articles/urban-soil-sealing-in-europe>

Zêzere, J. L., Pereira, S., Tavares, A. O., Bateira, C., Trigo, R. M., Quaresma, I., Santos, P. P., Santos, M., Verde, J. (2014). DISASTER: a GIS database on hydro-geomorphologic disasters in Portugal, Springer Science+Business Media Dordrecht.

Annex C - Flood discharge tunnel's mouth's technical drawing

